Title: Distinct function of SPL genes in age-related resistance in *Arabidopsis*

Lanxi Hu[1], Peng Qi[2], Alan Peper[1], Feng, Kong[1], Yao Yao[3], Li Yang[1]*

Affiliations**:**

1. Department of Plant Pathology, College of Agricultural & Environmental Sciences, University of Georgia, Athens, GA, 30602, USA

2. Department of Plant Biology, Franklin College of Arts and Sciences, University of Georgia, Athens, GA, 30602, USA

3. Department of Animal and Diary Sciences, College of Agricultural & Environmental Sciences, University of Georgia, Athens, GA, 30602, USA

* corresponding author

Abstract:

In plants, age-related resistance (ARR) refers to a gain of disease resistance during shoot or organ maturation. ARR associated with vegetative phase change, a transition from juvenile to adult stage, is a widespread agronomic trait affecting resistance against multiple pathogens. How innate immunity in a plant is differentially regulated during successive stages of shoot maturation is unclear. In this work, we found that *Arabidopsis thaliana* showed ARR against its bacterial pathogen *Pseudomonas syringae pv. tomato* DC3000 during vegetative phase change. The timing of the ARR activation was associated with a temporal drop of miR156 level. A systematic inspection of the loss- and gain-of-function mutants of 11 *SPL* genes revealed that a subset of *SPL* genes, notably *SPL2*, *SPL10*, and *SPL11,* activated ARR in adult stage. The immune function of SPL10 was independent of its role in morphogenesis. Furthermore, the SPL10 mediated an age-dependent augmentation of the salicylic acid (SA) pathway partially by direct activation of *PAD4*. Disrupting SA biosynthesis or signaling abolished the ARR against *Pto* DC3000. Our work demonstrated that the miR156-SPL10 module in *Arabidopsis* is deployed to operate immune outputs over developmental timing.

Significance

Age-associated change of immunity is a widespread phenomenon in animals and plants. How organisms integrate immune maturation into a developmental clock is a fundamental question. Heterochronic microRNAs are key regulators of developmental timing. We found that a conserved heterochronic microRNA (miRNA) in *Arabidopsis*, microRNA156, regulates the timing of age-related resistance associated with a transition from the juvenile to the adult vegetative phase. The coordination between developmental maturation and gain of disease resistance is achieved through miR156-controlled SPL transcription factors with distinct functions. A subset of SPL transcription factors promoted resistance by directly activating key genes in defense signaling. This work bridges the knowledge gap between vegetative development and age-related resistance. Pinpointing mechanisms of the developmental regulation on immunity may pave a way for unlocking the age limit on plant immunity and lay a foundation to applications in the precision agriculture.

Introduction

Both animals and plants suffer from infectious diseases, particularly at a young age (1-3). The function of their immune systems can be enhanced with the progression of organismal maturation. In many plant species, a gain of disease resistance against certain pathogens during shoot maturation is termed age-related resistance (ARR). Plant ARR can launch robust and wide spectrum resistance against a variety of pathogens, and such trait is often selected in breeding (4).

Age-associated disease resistance is often coupled with successive developmental transitions, such as germination (5) and vegetative phase change (6) and flowering (7, 8). The heterogeneity of host age, maturing stage of infected organs and virulence of causal pathogens suggest that multiple layers of signaling are intertwined between aging and immunity (4, 9). ARR-associated juvenile-to-adult vegetative phase change (hereafter ARR_{VPC}) has been observed among economically important vegetables, crops and fruits, such as tomato, rice and grapevine (10). The juvenile and adult phases refer to vegetative development prior to floral induction, and predicable changes of morphological and physiological traits are associated with this transition (11-13). Several factors were speculated to impact ARR_{VPC}. Compared to juveniles, adult plants are exposed to environmental conditions that are not optimal for disease development (such as high UV) (3); adult tissues may carry tough physical barriers (e.g., cell wall components, cuticle) (14); and leaves of adult stage are primed by previous exposure to pathogens (3). Such factors complicate the investigation of intrinsic molecular mechanisms governing the onset of ARR_{VPC}. Nevertheless, accumulating evidence suggests that intrinsic signaling pathways govern ARR (4, 15).

MicroRNA156s (miR156), a conserved microRNA family (11), regulates the onset of vegetative phase change (11, 16). MiR156 targets genes encoding SPLs (SQUAMOSA PROMOTER BINDING PROTEIN-LIKE) transcription factors, which

112 contains a SQUAMOSA promoter binding protein (SBP) box for nuclear import and
113 DNA binding (17-19). In *Arabidopsis*, leaves generated in the juvenile shoot, e.g.,
114 juvenile leaves (usually leaves 1-7 under a short-day condition) accumulate high level
115 of miR156 (20, 21). Throughout the expansion of juvenile leaves, they maintain the
116 morphological (e.g. no abaxial trichome) and molecular identities (e.g., high miR156
117 level) of the juvenile fate. A temporal decline of miR156 level, followed by the high
118 expression of *SPL*s, initiates the vegetative phase change (19-22). SPLs have
119 overlapping yet distinct functions to promote adult traits such as adult leaf
120 morphogenesis, floral induction, and reduced rooting (23-25). A total of 11 *SPL* genes
121 encoded in *Arabidopsis* Columbia-0 (Col-0) ecotype are suppressed by miR156 via
122 mRNA cleavage and/or translational repression (19, 26). Recent studies showed that
123 the miR156-SPL pathway involved in plant immunity. Disrupting miR156 function in
124 *Arabidopsis* by mutating SQUINT (SQN), an *Arabidopsis* orthologue of cyclophilin 40,
125 compromised jasmonic acid signaling and disease resistance against necrotrophic
126 pathogen *Botrytis cinerea* (27). Furthermore, overexpressing miR156-targeted *SPL9*
127 in juvenile plants enhanced accumulation of reactive oxygen species and induced
128 salicylic acid (SA) signaling, leading to enhanced resistance of *Arabidopsis* against
129 bacterial pathogen *Pseudomonas syringae* (28). Yet, a systematic dissection of the
130 link between ARR and miR156-SPL signaling pathway is still lacking.
131
132 Here, we systemically analyzed the miR156-SPLs module in ARR_{VPC}. We
133 demonstrated that the ARR to *Pseudomonas syringae pv. tomato* DC3000 (*Pto*
134 DC3000) in *Arabidopsis* is associated with vegetative phase change. Altering the
135 temporal expression of miR156-SPL pathway was sufficient to change the timing of
136 ARR_{VPC} onset. A sub-class of SPL transcription factors (SPL2/10/11) promoted
137 disease resistance in adult stage, and such function was independent of their roles in
138 leaf morphology. Transcriptomic analysis unveiled multiple mechanisms that
139 collectively contribute to ARR_{VPC}, including priming, activating adult-specific defense

140 programs, and strengthening juvenile defense after infection. Finally, we found SPL10
141 strengthened SA signaling in the adult stage by directly enhancing the transcription of
142 PAD4. Our work provides molecular insights into the intrinsic clock that coordinates
143 disease resistance outcomes with developmental timing.
144
145 **Results**
146 **The age-related resistance to *Pto* DC3000 is associated with a reduction of**
147 **miR156 level**
148
149 To assess the ARR_{VPC}, we measured the multiplication of *Pto* DC3000 in juvenile
150 (without abaxial trichomes) and adult (with abaxial trichomes) leaves of *Arabidopsis*
151 *thaliana* Col-0 ecotype. During the expansion of an individual leaf, defense gene is
152 differentially expressed (SI Appendix, Fig. S1), which is known as ontogenic
153 resistance (5, 29-32). Ontogenic resistance occurs during the maturation of both
154 juvenile and adult leaves (SI Appendix, Fig. S1). Because juvenile leaves are
155 produced in early shoot development, juvenile and adult leaves on a same plant are
156 always at different ontogenic age (SI Appendix, Fig. S1). To avoid the impact of
157 ontogenic resistance, we sampled fully expanded juvenile leaves (leaves 1-4) and
158 adult leaves (leaves 8) from 5-, 6- and 7-week-old plants, respectively. To avoid the
159 influence of flowering-associated ARR (33, 34), plants were grown in a
160 short-day condition and bolting was not observed before 10 weeks after
161 planting. Bacterial multiplication in leaves 8 was lower than that in leaves 1, 2, 3 and 4
162 (Fig. 1 A and B, and SI Appendix Table S2). No significant differences were observed
163 between leaves 1-2 and 3-4 (Fig. 1 B). We concluded that the increased resistance to
164 *Pto* DC3000 was associated with vegetative phase change in Col-0.
165
166 Since miR156 level in fully expanded leaves drops from the juvenile to adult transition
167 (35), we hypothesized that a high level of miR156 suppresses immunity in juvenile

168 stage. We compared bacterial growth in adult leaves (leaves ≥ 8) from Col-0 and
169 leaves at the same position from transgenic plants overexpressing *MIR156A* under a
170 constitutive 35S promoter from TMV (*35S::MIR156A*). Expressing *MIR156A* in adult
171 leaves led to accelerated production of juvenile leaves, marking the prolonged
172 juvenile phase as previously reported (20, 21) (Fig. 1 C). Interestingly, it also led to an
173 increase in bacterial growth when compared with leaves at the same position in Col-0
174 (Fig. 1 D). Consistently, knocking down miR156 activity by a target mimicry,
175 35S::*MIM156* (36) (*MIM156*) displayed enhanced disease resistance (Fig. 1 E and
176 F). These evidences suggests that high accumulation of miR156 suppresses
177 resistance to *Pto* DC3000 in the juvenile phase.
178
179 **miR156-regulated SPL10 promotes ARR in adult phase.**
180
181 To test which miR156-targeted *SPL* contributes to ARR_{VPC}, we first screened disease
182 phenotype in the gain-of-function mutants among 9 available (out of 11)
183 miR156-targeted SPLs (Fig. 2 A and SI Appendix, Table S2). We examined the
184 disease phenotype in juvenile leaves expressing individual miR156-resistant *SPL*
185 gene under its own native promoter (*rSPLs*) (24). Low levels of endogenous *SPL*
186 transcripts in juvenile leaves provided a sensitized background to test the function of
187 *rSPLs*. We found that leaves 1-2 from *rSPL2*, *10*, *9* and *13* showed increasing
188 resistance compared to wild type, but *rSPL3*, *4*, *6*, *11* and *15* did not change
189 resistance to *Pto* DC3000 (Fig. 2 A and SI Appendix, Table S2 and Figure S2). Thus,
190 a subset of miR156-regulated SPLs was sufficient to enhance immunity in juveniles.
191
192 To check the necessity of SPLs in adult conferred immunity, we tested disease
193 phenotypes in adult leaves with loss of function *spl* combinatorial mutants based on
194 amino acid sequence similarity (Fig. 2 A; SI Appendix, Table S2 and Figure S2).
195 There are 5 phylogenic clades for miR156-targeted *SPL* genes, *SPL3/4/5*, *SPL6*,

196 *SPL2/10/11*, *SPL9/15*, and *SPL13A/13B* (Fig. 2 A) (26, 37). In Col-0 background,
197 *SPL10* and *SPL11* (78% amino acid identity) reside in a 1.6 kb tandem duplication
198 (26). S*pl2/10/11* showed enhanced susceptibility to *Pto* DC3000 (Fig. 2 A). While the
199 phenotypes of *spl2 and spl10* single mutants were wild type-like, *spl10/11* mildly
200 reduced disease resistance (SI Appendix, Table S2), indicating that *SPL2, 10* and *11*
201 redundantly contributed to immunity in adult leaves. Importantly, although *rSPL10*
202 carried a higher resistance than wild type in juvenile leaves (Fig. 2 A and B), the
203 difference between the two genotypes was much smaller in the adult stage (Fig. 2 B),
204 supporting that SPL10 enhanced resistance is age dependent. *Spl3*/*4*/*5* triple or *spl6*
205 single mutations did not alter resistance to *Pto* DC3000 (Fig. 2 A; SI Appendix, Table
206 S2). The lack of disease phenotypes against *Pto* DC3000 in the gain- and
207 loss-of-function mutants of *SPL6* is consistent with a previous report (38). *rSPL9*
208 enhanced resistance, but the *spl9/15* double mutant displayed unstable phenotypes,
209 which may be resulted from redundancy among other SPL members (Fig. 2 A and SI
210 Appendix, Table S2). Altogether, the data confirmed the specialized function of SPLs
211 in ARR_{VPC}.
212
213 To further determine whether the disease phenotypes of *SPL10* mutants were
214 pleiotropic effects caused by SPL10-mediated leaf morphogenesis, we assayed
215 bacteria multiplication in transgenic plants expressing either estradiol inducible *rSPL3*,
216 *rSPL10* or *MIM156* (Fig. 2 C). Transgenic plants growing on ½ MS medium
217 supplemented with estradiol showed typically early phase change phenotypes,
218 indicating that the transgenes were functional (24, 39). In line with the data above (Fig.
219 2A), applying estradiol 12 hrs before inoculation suppressed bacterial multiplication in
220 juvenile leaves of inducible *rSPL10* and inducible *MIM156* lines, but not for that from
221 inducible *rSPL3* plants (Fig. 2 D). Notably, the leaf morphology was comparable
222 between wild type and estradiol induced plants (Fig. 2 C), indicating that
223 miR156-SPL10 controlled disease resistance and leaf morphology can be decoupled.

224

225 **The basal expression of defense genes is high in the adult stage.**

226

227 To explore the transcriptional signature of ARR_{VPC}, we performed RNA sequencing to
228 compare juvenile (leaves 1-2) and adult (leaves ≥ 8) transcriptomes at 3 hours after
229 mock treatment or *Pto* DC3000 infection (Fig. 3 A). An early time point was chosen
230 because change of chromatin accessibility could be detected at 3 hrs post *Pto*
231 infection (40). Under mock treatment, we identified 2002 and 2320 genes that were
232 respectively up- or down-regulated in adult leaves compared with juvenile leaves,
233 hereafter $Adu_{no\ infection\ (nof)}$ (LFC = 0.58, padj < 0.05) (Fig. 3 B, and SI Appendix, Table
234 S3 and Figure S3 C and S3 D). As expected, *SPL3/4/5* were up-regulated in adult
235 samples (SI Appendix, Table S3). In addition, the Gene Ontology (GO) enrichment
236 analysis revealed that vegetative phase change related GOs, such as adaxial/abaxial
237 axis specification (41) were enriched in the Adu_{nof} DEGs (Fig. 3 D and SI Appendix,
238 Table S6.1), confirming that our juvenile and adult samples represented two distinct
239 developmental phases (SI Appendix, Fig S3 A-B and SI Appendix, Table S3).
240 Intriguingly, we observed that immunity related GOs were also enriched in the
241 up-regulated Adu_{nof} DEGs, including defense response to bacterium/fungus and
242 response to SA (Fig. 3 D). Here, jasmonic acid (JA) signaling-mediated defense was
243 downregulated, coinciding with the antagonistic interaction between JA and SA in
244 plant immunity (42). The enrichment of pro-defense genes in up-regulated Adu_{nof}
245 indicated that adult plants had primed defense signaling.

246

247 For defense induction state, we investigated genes that were differentially
248 induced/suppressed by infection in juvenile and adult stages. *Pto* treatment triggered
249 3027 and 4728 DEGs in juvenile and adult leaves, respectively (SI Appendix, Table
250 S3-S4 and Fig S3 C and S3 D). Among the 2163 *Pto*-triggered DEGs shared between
251 juvenile and adult leaves (2163 = 239 + 1924 in Fig. 3 C and SI Appendix, Table

252 S3-S4 and Fig S3 C and S3 D), the shared up-regulated DEGs were enriched with
253 well-characterized defense responses such as respiratory burst, defense response to
254 bacterium and response to salicylic acid (Fig. 3 D). Meanwhile, photosynthesis and
255 light harvesting signaling pathways were enriched in down-regulated DEGs, indicating
256 that a pathogen-induced transcriptomic reprogramming switched from development to
257 defense regardless of plant age (Fig. 3 D, SI Appendix, Table S6.1). A total of 864
258 DEGs were only induced/repressed by *Pto* in the juvenile stage, and there are 2565
259 DEGs were adult-specific (Fig. 3 C). Cutin biosynthetic and wax biosynthetic
260 processes were enriched in adult-specific *Pto*-induced DEGs, consistent with a
261 previously suggested consolidation of constitutive defense in ARR (43) (SI Appendix,
262 Table S6.2).
263
264 We noticed that a portion of genes specifically induced in the adult stage did not
265 eventually have higher transcription level than those in juvenile stage. It is arguable
266 whether inducibility of a gene alone contributes to ARR. So, we further searched for
267 genes whose absolute expression levels were different between juvenile and adult
268 leaves after *Pto* DC3000 treatment (hereafter Adu_{pto}). Genes that were specifically
269 induced/repressed by infection in the adult stage count for 20.6% (934 out of 4528, SI
270 Appendix, Table S3) of the Adu_{pto} (Fig. 3 C). There, cellular response to hypoxia,
271 defense response to bacterium and response to heat were over-represented,
272 indicating an age-dependent *Pto* response that may cope with abiotic stresses (Fig. 3
273 D). A 5.3% (239 out of 4528, SI Appendix, Table S3) of Adu_{pto} were also triggered by
274 *Pto* in the juvenile stage, but the amplitude of change was preferentially higher in the
275 adult stage (Fig. 3 C). Thus, ARR_{VPC} strengthened a sector of juvenile-defense
276 regulon as well as activated adult-specific defense genes. In addition, 38% (1722 out
277 of 4528) of Adu_{pto} were not *Pto*-triggered but already had differential expression
278 between juvenile and adult leaves before infection (Fig. 3 B, SI Appendix, Table S3).
279 Of the 38%, GOs pertaining to defense, such as SA signaling, together with

280 adult-related developmental pathways were enriched (Fig. 3 D, SI Appendix, Table
281 S6.1). Finally, 20.1% Adu_{Pto} (910 out of 4528) was not induced either by infection or
282 age alone. These DEGs could be resulted from a synergistic interaction between age
283 and infection (Fig. S3 C and SI Appendix, Table S3). Taken together, we discovered
284 that ARR transcriptome changes could contribute to the elevation of defense signaling
285 at non-infected state, the adult-specific inducible defense as well as the strengthened
286 juvenile defense.
287
288 **Overexpressing SPL10 recapitulates the ARR transcriptomic landscape in**
289 **juvenile leaves.**
290
291 To delineate the contribution of SPL10 to ARR at the transcriptomic level, we
292 investigated the *rSPL10 (r10)* induced DEGs at non-infected and *Pto*-infected states
293 (Fig. 3 A). A total of 3211 genes (1859 up-regulated and 1352 down-regulated) were
294 differentially expressed in leaves 1-2 between Col-0 and *r10* at non-infected state
295 ($r10_{nof}$). Among them, 936 out of 3211 $r10_{nof}$ DEGs were co-regulated in adult leaves,
296 attributing to 21.7% (936/4322) of the Adu_{nof}, being consistent with the function of
297 SPL10 in specifying adult fate (Fig. 4 A, SI Appendix, Table S5). GO terms associated
298 with immune signaling including systemic acquired resistance were enriched in the
299 936 co-upregulated DEGs between $r10_{nof}$ and Adu_{nof} (Adu/$r10_{nof}$) (Fig. 4 C, SI
300 Appendix, Table S6.3). After bacterial infection, we identified 2621 DEGs between
301 leaves 1&2 from *r10* and Col-0. 604 of those DEGs were also Adu_{pto}, occupying
302 13.3% (604/4528) of total Adu_{pto} (Adu/$r10_{Pto}$) (Fig. 4 B, SI Appendix, Table S5).
303 Defense-related GOs were enriched in those co-regulated DEGs (Fig. 4 C, SI
304 Appendix, Table S6.3). The observations support that SPL10 activated a sector of
305 adult immune response to *Pto* DC3000.
306
307 **Disrupting SA signaling compromised the SPL10-mediated ARR.**

308

309 Since SA-related GO terms were enriched in the co-upregulated Adu/*r10*$_{nof}$ (Fig. 4 C),
310 we first measured the age- and SPL10- effects on SA signaling. We assembled a core
311 SA regulon by overlapping DEGs induced by SA and its synthetic inducer
312 benzothiadiazole (BTH) (44, 45) (Fig. 5 A). 81.3% of the core SA regulon (527
313 activated and 239 repressed genes) were detected in our sequencing data.
314 SA-activated (199/527) and -repressed (50/239) markers were enriched in Adu$_{nof}$ (Fig.
315 5 B and SI Appendix, Information S6). SA-activated genes were also enriched in *r10*$_{nof}$
316 (Fig 5 B and SI Appendix, Information S6), denoting that SPL10 contributed to
317 enhancing SA signaling in the adult phase. Consistently, accumulation of Salicylic
318 acid beta-glucoside (SAG) (an inactive SA form, stored in vacuole) was higher in adult
319 than that in juvenile leaves (Fig. 5 C and SI Appendix, Table S2). The accumulation of
320 free SA showed a similar trend (Fig. 5 C and SI Appendix, Table S2). Next, we sought
321 to validate whether elevated SA response in adult phase depended on the temporal
322 expression of *SPL10*. We selected four age-dependent SA-activated genes,
323 *AT3G60470, BG3, ATLTP4.4* and *PR5*. Their expressions were compromised in the
324 adult leaves of *spl2/10/11* (Fig. 5 D). Noticeably, the upregulation of the four SA
325 responsive genes were also observed in adult or *r10* leaves when plants were grown
326 on sterile plates (Fig. 5 E). In conclusion, the age-related increase of SA response in
327 leaves required *SPL10*, and was not primed by pre-exposure to microbes. The
328 EDS1-PAD4 protein complex is essential for SA-mediated defense signaling (46). We
329 found that both genes were upregulated in adults and *r10* (Fig. 4 A). Furthermore, a
330 significant overlap was found between the EDS1-PAD4 core regulon (EP-core, (46)
331 and genes co-upregulated by adults and *r10* (Fig. 5 F), implying that the EDS1-PAD4
332 mediated SA signaling pathway could be differentially activated in juvenile and adult
333 stage due to the temporal expression of SPL10.

334

335 Out of the 936 DEGs co-regulated by adult stage and *rSPL10* (Fig. 4 A), 400 of them
336 were associated with SPL10-binding sites identified in a ChIP-seq experiment of
337 SPL10 by Ye *et al* (Fig. 6 A) (25), indicating that these genes are likely direct targets
338 of SPL10. A de novo motif discovery algorism identified potential SPL-binding sites in
339 203 of the co-up-regulated DEGs (Fig. 6 A), but not in the 197 down-regulated genes.
340 In addition, experimentally validated SPL TF binding sites (47) were enriched in the
341 promoter of the 203 genes (SI Appendix, Fig S5 A). Interestingly, the promoter region
342 and gene body of *PAD4* contains two potential SPL10-binding GTAC-containing
343 motifs (Fig. 6 B) (25). We generated a genomic reporter line of SPL10
344 (*proSPL10::rSPL10-YFP*). The transgenic line showed similar early phase change
345 phenotypes observed in the *proSPL10::rSPL10-GUS* line, indicating that the fusion
346 had a normal SPL10 function (SI Appendix, Fig S5 B). Using ChIP-qPCR, we
347 validated that the motif 1 (M1, 186-182 bp away from the TSS), but not motif 2 was
348 associated with SPL10 at uninfected state (Fig. 6 B). Furthermore, the transcript level
349 of *PAD4* was reduced only in the *spl2/10/11* adult leaves but not in the juvenile leaves
350 (Fig. 6 C), indicating that the temporal expression of *PAD4* depends on SPL10. Taken
351 together, these observations suggest that SPL10 directly promotes *PAD4* expression
352 in the adult stage.
353
354 To probe the genetic interactions of SA signaling and the miR156-SPL10 mediated
355 ARR, we first tested the ARR_{VPC} phenotype in the mutant of *SALICYLIC ACID*
356 *INDUCTION DEFICIENT 2* (*sid2-1*, defective in pathogen-induced SA biosynthesis)
357 and *NONEXPRESSER OF PR GENES 1* (*npr1-1*, defective in SA perception)
358 mutants. Neither of those mutants altered the timing of vegetative phase change. As
359 expected, both mutants in adult stage were more susceptible than Col-0 (Fig. 7 A).
360 The difference of bacterial growth between wild type and the mutants in juvenile stage
361 was less pronounced (Fig. 7 A), in agreement with the age-dependency of
362 SA-mediated disease resistance. We then introduced *sid2-1* mutation into *MIM156*

363 background (SI Appendix, Fig. S5 A). Although precocious morphological traits were
364 shared between *MIM156* and *MIM156/sid2-1*, the bacteria level in *MIM156/sid2-1*
365 phenocopied that of *sid2-1* (Fig. 7 B), suggesting that *SID2* acts downstream of
366 miR156. Similarly, loss of function mutation of *EDS1* reversed the enhanced disease
367 resistance phenotype in *r10* plants (Fig. 7 C, SI Appendix, Fig. S5 B). The leaf
368 morphology phenotype of *r10* plants was not changed by *eds1.2*, which further
369 confirmed that age-associated leaf morphology and disease resistance can be
370 decoupled (Fig. 7 C). Consistent with the molecular evidence that SPL10 binds to the
371 promoter of *PAD4*, the ARR_{VPC} phenotype was compromised in *pad4-1* and *eds1.2*
372 mutant (Fig. 7 D). In essence, miR156-SPL10 promoted resistance through *SID2* and
373 *EDS1-PAD4*-dependent SA signaling.
374

375 **Discussion**

376 In this research, we uncovered an ARR mechanism regulated by the miR156-SPL
377 pathway, linking immune maturation to an intrinsic aging mechanism (SI Appendix,
378 Fig. S6). In plants, ARR occurs during predicable developmental transitions that are
379 often accompanied by morphological changes. Our research provides a potential
380 mechanism for the temporally coordinated change of immunity and morphogenesis,
381 where the same molecular clock, miR156, controls different *SPL* genes to specify
382 immune and developmental traits. For instance, SPL2/10/11, but not SPL3/4/5/6, are
383 required for resistance against *Pto* DC3000 (Fig. 2 A). Interestingly, NbSPL6 is
384 required in the N-mediated TMV resistance in tobacco (38). The homologue
385 of *NbSPL6* in *Arabidopsis*, *AtSPL6*, is necessary to the full ETI response triggered
386 by *Pseudomonas syringae* effector AvrRps4, but not basal resistance to *Pto* DC3000
387 (38) (Fig. 2 A). It is possible that the broad spectrum of resistance associated with
388 ARR requires multiple SPL family members to activate different defense pathways. As
389 rSPL10 only influenced 21.7% of Adu_{nof} and 13.3% of Adu_{pto}, other SPLs may
390 contribute to the rest of adult defense to *Pto* and/or to other pathogens (Fig. 4 A and 4

391 B). Alternatively, the coordinated maturation of development and immune system may
392 be achieved by functional switch of the same SPL protein. In rice plants, *Ideal plant*
393 *architecture 1* (*IPA1*)/*OsSPL14* and *OsSPL7* promote growth in a non-infection status.
394 It binds to an alternative cis-regulatory element to activate defense when challenged
395 by the bacterial pathogen *Xanthomonas oryzae pv. Oryzae* (*Xoo*) (48, 49).
396 In *Nicotiana benthamiana* and tomato plants, temporal reduction of miR6019/6020
397 allows its target, *N* gene, to mediate age-dependent resistance to tobacco mosaic
398 virus (TMV) (50). The temporal expression pattern of miR6019/6020 mimics that of
399 miR156 in tobacco. It would be interesting to explore the genetic relationship between
400 those two miRNAs in regulating ARR.
401
402 We showed that defense GO terms were enriched in up-regulated *rSPL10*$_{nof}$ and
403 Adu$_{nof}$. Among those, components of SA pathway, such as *SID2* and *NPR1* were
404 required for ARR$_{VPC}$ (Fig. 6). We observed the up-regulation of SA response
405 accompanied by a reduction of JA response in both Col-0 adults and the *rSPL10* line
406 (Fig. 3 and 4). JA and SA often act antagonistically to fine-tune immune response to
407 multiple pathogens. Our ARR transcriptome results showed that the antagonism also
408 occurred in an age-dependent manner (Fig 3 C). Upregulation of SA production and
409 response have also been observed during vegetative-floral transition in both tomato
410 and tobacco plants (51). In *Arabidopsis*, *SVP* and *SOC1* genes regulating floral
411 induction also transcriptionally promote age-dependent increase of SA, independent
412 from flowering traits (52, 53). We did not observe differential expression of *SVP* or
413 *SOC1* in juvenile *vs* adult transcriptome, suggesting the *SVP-SOC1* module may not
414 act in the ARR$_{VPC}$ of *Arabidopsis*. On the other hand, we found that ARR$_{VPC}$ was
415 *NPR1*-dependent (Fig. 6 A), which is different from an age- and SA-associated but
416 *NPR1*-independent gain of resistance observed before (54). It is likely that there are
417 parallel aging pathways strengthen SA signaling during plant maturation.
418

419 In co-upregulated Adu/*r10*$_{pto}$ DEGs, we noticed that cellular response to hypoxia was
420 enriched (Fig. 4 D). Response to hypoxia of plants has been reported for
421 counteracting submergence and waterlogging stress (55). Respiratory burst, as part
422 of immune responses, is oxygen dependent. At the site of *Botrytis cinerea* infection,
423 hypoxic response was induced, leading to the stabilization of subgroup VII of
424 ETHYLENE RESPONSE FACTOR (ERF-VII) (46). Members in the ERF-VII can
425 activate defense gene as well as hypoxic response (46). SPL10 may upregulate
426 genes that react to low-oxygen environment when reactive oxygen species
427 accumulates or respiration increases. How hypoxia response contributes to ARR
428 against biotrophs and necrotrophs remains to be seen.
429
430 Plant innate immunity shares similarities to human innate immunity, ranging from
431 structures and functionality of innate immune receptors and their downstream
432 signaling cascades (56, 57). Our discovery of miR156-SPL signaling in ARR$_{VPC}$
433 provides further evidence that heterochronic miRNAs coordinate aging and immunity
434 *in planta*. In *Caenorhabditis elegans*, *let-7* family microRNAs are well-characterized
435 regulators of developmental timing by specifying stage-specific cell fates in the
436 hypodermal seam cell lineages (58, 59). Interestingly, let-*7-fam* miRNAs also repress
437 the worm's resistance to *Pseudomonas aeruginosa*, an opportunistic human pathogen
438 (60). The dual function of *let-7-fam* in developmental timing and immunity is fulfilled
439 through integrating downstream heterochronic genes and the p38 MAPK pathway
440 (60). Thus, deploying heterochronic microRNAs pathway can be a cross-kingdom
441 strategy to integrate immunity and developmental timing. It will be exciting to further
442 dissect the genetic components and regulatory architecture of coordinated maturation
443 of immunity and development.
444
445 **Material and methods**
446

447 **Plant material and growth conditions**

448 *Arabidopsis* wild type, transgenic lines and mutants used in this study were in a
449 Columbia-0 (Col-0) genetic background unless mentioned otherwise. The genetic
450 cross of *MIM156/sid2-1* and *r10/eds1.2* were generated from this research and
451 progenies from F3 or F4 generation were used for phenotypic test. Information for
452 mutants and transgenic lines can be found in SI Appendix, Table S1. Juvenile leaves
453 were fully expanded leaves 1-2, or 3-4 from soil-grown 5-week-old plants. Adult
454 leaves were fully expanded leaves that derived from 7-week-old plants. The adult
455 phase of a leaf was confirmed by appearance of abaxial trichomes (41). Plants were
456 sown on Fafard #3 Mix propagation soil. The planted seeds were then placed under
457 4 °C for 2 days and transferred to a growth room under 23°C/19°C day/night and with
458 45% humidity. Nine hours light and 15 hours dark photoperiod with
459 180 μmol $m^{-2}s^{-1}$ was used as short-day condition. Lighting was made through a 5:3
460 combination of white (USHIO F32T8/741) and red-enriched (interlectric F32/T8/WS
461 Gro-Lite) fluorescent lights. Plant age was counted from the first day when seeds
462 transferred to the growth room. Only plants used for Fig 5 E were grown on ½ MS
463 plates in 24h with continuous light.

464

465 **Sampling strategy for studying ARR_{VPC}**

466 In our short-day growth condition, plants produced 50-60 leaves before bolting. The
467 ontogenic age of a leaf influenced defense gene expression (SI Appendix, Fig. S1 A).
468 To minimize the influence of ontogenic age of individual leaves (SI Appendix, Fig. S1
469 B), we measured the expansion rate of juvenile and adult leaves and harvested fully
470 expanded juvenile and adult leaves from plants of different ages (SI Appendix, Fig. S1
471 C). Fully expanded leaves 1-4 derived from a 4- or 5-weeks old plants were sampled
472 as juvenile leaves; fully expanded leaves (range from 8-13 depending on variations in
473 plants) from 7-weeks old plants were sampled as adult leaves. Adult leaves showed
474 characteristic abaxial trichome(s), blade serration and elongated petiole (21). Plants

475 for adult samples were planted 2-3 weeks earlier than those for juvenile leaves.
476 Juvenile and adult samples were collected at the same time for disease assay and
477 transcriptome analysis.
478
479 **Bacterial growth assay**
480 *Pto* DC3000 strain was grown under 28°C on King's B solid medium (40 g/L proteose,
481 20 g/L glycerol and 15 g/L agar). The medium contained rifamycin for selection and
482 cycloheximide to inhibit fungi growth. Glycerol stock of the bacterial strains stored
483 under -80°C. Bacterial stock was streaked on plate for a 2-day growth and was
484 re-streaked one day before inoculation. For infiltration, bacteria were collected from
485 the plate and suspended in 10 mM $MgCl_2$ solution. Bacterial suspension with
486 concentration of 1 x 10^5 CFU/mL was infiltrated in *Arabidopsis* leaves with a needless
487 syringe. After inoculation, plants were covered by transparent lids for one hour. Day 0
488 samples were collected immediately after removing lids. Each sample contained four
489 leaf discs that were derived from four individual leaves. Leaf samples were collected
490 using the corer (the same size for all plants) and ground with homogenizer (OMNI
491 International) and diluted serially. KB plates with 10 µL of bacteria suspension per
492 sample were placed under room temperature for 2 days. Colony forming units were
493 counted manually and normalized according to inside area of the corer. Day 2
494 samples were collected as described above two days post-infiltration (dpi).
495
496 **RNA sequencing and analysis**
497 *Pto* DC3000 (1 x 10^8 CFU/mL suspended in 10mM $MgCl_2$) was infiltrated into juvenile
498 and adult wild type (Col-0) leaves and leaves 1-2 from *rSPL10* plants. 10 mM $MgCl_2$
499 was used as the mock treatment. Three hours after inoculation, 20 leaf discs with
500 comparable size from 5-10 individual plants were cored and collected as one biological
501 repeat per genotype per treatment. Three biological repeats were prepared for each
502 genotype/treatment. For RNA isolation, plant tissues were flash-frozen in liquid

503 nitrogen and then ground to fine powders using homogenizer (OMNI International).
504 Total RNAs were extracted using E.Z.N.A. Total RNA kit (Omega BIO-TEK). RNA
505 quality was assessed with a 2100 Bioanalyzer instrument (Agilent, RIN score ≥ 7,
506 28S/18S ≥ 1). RNA concentration was measured using a Nanodrop
507 spectrophotometer (Thermo Scientific, RNA concentration ≥ 50 ng/μL, 260/280 ~2.0).
508 RNA samples were sequenced at BGI San Jose lab. Oligo dT based mRNA
509 enrichment was followed by random N6 primer based reverse transcription. The
510 synthesized DNA nanoballs were then sent for strand-specific mRNA sequencing
511 (PE100) on a DNA Nanoball Sequencing (DNBseq) platform. The data was filtered
512 using SOAPnuke software in BGI. ~48 M clean reads with average Q30 ≥ 88.81% per
513 sample were obtained.
514
515 Files of RNA-seq raw reads together with processed data were uploaded to NCBI with
516 access No. GSE208657. The clean RNA-seq data were aligned against the TAIR10
517 reference genome using HiSAT2 (v.2.1.0, (61)) with following parameters, hisat2 -p 4
518 -x TAIR10indexed -1 sample_strand1.fq.gz -2 sample_strand2.fq.gz -S
519 aligned_sample.sam. The aligned reads were assembled into transcripts according to
520 the TAIR10 annotation (62, 63) using Stringtie (64). ~ 99% overall alignment rate was
521 reached for each sample. Differential expression analysis was done by comparing
522 transcript levels between pairwise normalized samples using DEseq2 package in R
523 (LFC ≥ ±0.58, padj ≤ 0.05) (65). Gene ontology was analyzed first against the whole
524 *Arabidopsis* genome at TAIR Gene Ontology terms website, http://geneontology.org/
525 (66, 67), and which was then confirmed using total detected 22,622 (covers 88.7% of
526 known genes in *Arabidopsis* genome) genes of the RNA-seq results on agriGO
527 website http://systemsbiology.cau.edu.cn/agriGOv2/# (68). Figures were generated in
528 R, with ComplexHeatmap package that was specifically used for Figure 3 B-D and 4
529 (69). Complete R scripts are available at SI Appendix, information S6.
530

531 **Motif discovery and enrichment analysis**

532 The de novo motif discovery analysis was carried on the website
533 (https://www.arabidopsis.org/tools/bulk/motiffinder/index.jsp). Frequencies of 6-mer
534 motifs were compared between 1000 bp upstream sequences of each input gene and
535 the current *Arabidopsis* genomic sequence set (33518 sequences). A total of 15
536 motifs containing the consensus SPL binding site, GTAC, were identified. A
537 frequency-based sequence logo was generated through the weblogo,
538 (https://weblogo.berkeley.edu/logo.cgi). To assess the enrichment of experimentally
539 validated TF binding sites, we used the SEA (https://meme-suite.org/meme/tools/sea).
540 1000 bp upstream sequences of the 203 Adu/*r10* co-upregulated DEGs (Fig. 6 A)
541 were extracted from TAIR. Shuffled input sequences were chosen as control
542 sequences. The DAP motif database (47) were selected to identify the enriched
543 motifs.

544

545 **qRT-PCR**

546 Bacterial suspension with 1 x 10^8 CFU/mL was infiltrated in *Arabidopsis* leaves. Leaf
547 samples were harvested at 3 hours hpi. Each sample had 16-20 leaf discs derived
548 from 6-10 individual plants. The leaf age of plants in soil was measured following the
549 same standard as the above. For plants on ½ MS plates, 15-20 leaves were
550 harvested per genotype per treatment as one biological rep. leaves 8-13 from
551 45-day-old of Col-0 with abaxial trichomes were used as adult leaves, leaves 1-2 from
552 18-day-old Col-0 were used as juvenile leaves. In comparison, leaves 1-2 from
553 21-day-old of *rSPL10* were used. For each bio-rep, three to six technical
554 replicates were used in one qPCR run. RNA extraction was performed
555 using Omega biotek EZNA plant RNA kit. The qPCR was performed in
556 the Applied Biosystems QuantStudio 1 Real-Time PCR system with SYBR Green
557 master mix (Applied Biosystems). PCR conditions were set as follows: 95°C for 5
558 mins, 40 cycles of 95°C for 15s, 56°C for 30s and 72°C for 20-30s. *SAND*

559 (*AT2G28390*) or *TUB2* (*AT5G62690*) was used as reference genes. The relative
560 expression was calculated using relative standard curve methods. Delta-delta CT was
561 also used for calculation when knowing that the PCR efficiency for the primers was at
562 least more than 95% in previous standard curve results. The oligonucleotides used
563 here can be found in SI Appendix, Table 1.
564
565 **Estradiol-induced gene expression**

566 The estradiol-inducible *MIM156* and *rSPL3* was constructed using a Gateway
567 compatible version of the XVE system, as described by Brand et al., (70).
568 The *MIM156* and *rSPL3* sequence were cloned into pMDC160. Transgenic plants
569 were crossed to plants containing pMDC150-35S (70) and generated homozygous.
570 The estradiol-inducible *rSPL10* was generated by cloning *rSPL10* into a modified
571 pMDC7 vector tagged with Citrine and HA.

572
573 **HPLC-MS**
574 Ten to sixty leaves 1-2 of Col-0 and *r10* each and three adult Col-0 leaves (plants
575 sawn in soil) were collected as one biological repeat for each genotype or a
576 developmental stage. 3 to 6 biological replicates from five (for adult tissues) to thirty
577 (for juvenile tissues) individual plants were collected in total. The leaves were then
578 lyophilized, powdered, and weighted for getting a comparable dry weight for all
579 samples (weighting error $\leq$ 0.1 mg). Metabolites from 1.5 mg or 8.5 mg (in separate
580 experimental repeats) of dry tissue of each biological replicate were extracted and
581 were detected under Liquid chromatography-mass spectrometry (HPLC-MS). Amount
582 of salicylic acid beta-glucoside (SAG) and salicylic acid (SA) were measured and
583 calculated in the unit of nmole metabolite per gram of dry weight (nmole/g DW).
584
585 **ChIP-qPCR assay**

586 The procedure and the preparation of reagents were modified from protocols (71-73) .
587 In brief, 1 gram of non-treated fully expanded adult leaf tissues were collected from
588 the pro*SPL10::rSPL10-YFP* line. Leaves from 2-3 plants were harvested as one
589 biological sample. Three biological replicates in total from two independent
590 experiments were used. The tissue was crosslinked, and the chromatin was extracted
591 and sonicated using nuclei extraction buffers and a bioruptor UCD-200 with chilling
592 pump. 15 µL of post-sonicating chromatin solution was saved as the input. The
593 remaining chromatin solution was immunoprecipitated by using GFP-trap Magnetic
594 Agarose (ChromoTek, cat no. gtma). Diluted input and DNA eluted after IP were used
595 for qPCR using primers at the indicated positions (Fig. 6 B; SI Appendix, Table 1). We
596 used the following formula to calculate the estimated CT value for adjusting CT values
597 of input and IP samples, ∆Ct [normalized ChIP] = (Ct [Input] – Log2 (dilution factor for
598 Input)) – ((Ct [ChIP] – Log2 (dilution factor for ChIP)), and the final output % input =
599 100 * 2 ^ (∆Ct [normalized ChIP] (73).
600
601 **GUS staining assay**
602 Plants carrying pro*PR2*::GUS were harvested at six week after planting. The GUS
603 solution was prepared as following and was vacuum infiltrated into plants, 0.1 M
604 $NaPO_4$, pH 7.0, 10 mM EDTA. 0.1% Triton X-100, 1 mM $K_3Fe(CN)_6$, 2 mM X-Gluc
605 (X-Gluc was dissolved in N ,N-DMF and made fresh). After 24 h incubation at 37°C, the
606 staining solution was replaced with 70% ethanol. Tissues were washed several times
607 with 70% ethanol until the chlorophyll in leaves was cleared. The GUS-stained leaves
608 were imaged using a dissecting microscope (VWR).
609
610 **Acknowledgement**
611 We thank Scott Poethig from University of Pennsylvania to provide *rSPL* and *spl*
612 mutants. We thank Khadijeh Mozaffari, Scott Harding and Chung-Jui Tsai of the Plant

613 Metabolomics Laboratory at the University of Georgia for analytical assistance. We
614 thank Jovana Mijatovic for providing feedback on the manuscript. Y.L. conceptualized
615 the project. Y.L. and H.L. designed experiments. H.L. performed experiments. P.A.
616 and K.F. participated repeating experiments in Figure 2 A and Figure 6 B, respectively.
617 H.L., Q.P. Y.Y and Y.L. analyzed data. H.L. and Y.L. wrote the manuscript. Funding for
618 the UPLC-Q-TOF was provided by the United States Department of Agriculture,
619 National Institute of Food and Agriculture, Equipment Grant Program award no.
620 2021-70410-35297. This project is supported by NIH R35GM143067 to Y.L.
621
622
623
624
625 **Figure 1. MiR156 suppressed age-related resistance to *Pto* DC3000 in**
626 ***Arabidopsis*. A**, developmental phenotype of a 4-week (left) and 7-week (right) Col-0
627 plant grown under short-day conditions. Arrows point to leaves 1,2,3,4 and leaf 8 in
628 the left and right plants, respectively. **B**, *Pto* DC3000 bacterial growth in juvenile and
629 adult leaves of Col-0. **C**, developmental phenotype of a 7-week Col-0 and
630 *35S::MIR156A* plant. Arrows indicate an adult leaf of Col-0 or a leaf from a similar
631 position in *35S::MIR156A*. **D**, bacterial growth in adult leaves of Col-0 and
632 *35S::MIR156A*. **E**, developmental phenotype of a 4-week Col-0 and *35S::MIM156*
633 plant. Arrows indicate leaves 1 and 2 on each plant. **F**, *Pto* DC3000 bacterial growth
634 in juvenile Col-0 and *MIM156* leaves 1-2 on Day 0 and Day 2. Scale bar = 1 cm. Day 0,
635 the day of *Pto* infection. Day 2, two days post-infection. CFU/cm^2, bacterial colony
636 forming unit per square centimeter of a leaf. Juv, juvenile leaves, Adu, adult leaves.
637 The student t-test was used for statistical analysis. Each genotype was compared with
638 Col-0, ns, not significant, *, $p < 0.05$, **, $p < 0.01$. The same annotation is used for
639 bacterial growth dot-box plots shown in Figures 2 and 7. Repeats of bacterial growth
640 are presented in SI Appendix, Table S2.

641

642 **Figure 2. MiR156-targeted SPL10 promoted resistance to *Pto* DC3000. A**, disease
643 phenotype of *Pto* DC3000 in *SPL* gain and loss-of function mutants. NA, not available.
644 **B**, bacterial growth in leaves 1-2 and leaves 11 from Col-0 and *rSPL10*. **C**,
645 developmental phenotype of Col-0, and early phase change phenotypes of transgenic
646 plants expressing stable *MIM156*, *rSPL10* and *rSPL3* on ½ MS plate (top panel);
647 developmental phenotype of Col-0, *estradiol-inducible(in)MIM156*, *inrSPL10* and
648 *inrSPL3* at 3 days after estradiol treatment (bottom panel). **D**, bacterial growth in
649 leaves 1-2 from 4 -week-old Col-0, *inMIM156*, *inrSPL10* and *inrSPL3* on Day 0 and
650 Day 3. Emmeans package in R was used for statistical analysis in 2 A and 2 B. The
651 student t test was used for statistical analysis in 2 A and 2 C, and each genotype was
652 compared with Col-0 wild type, ns, not significant, *, $p < 0.05$, **, $p < 0.01$. Repeats for
653 the experiments here are shown in SI Appendix, Table S2.

654

655 **Figure 3. Basal transcript level of defense genes were heightened over**
656 **vegetative phase change. A**, experimental settings of RNA-seq. Non-infected state
657 and challenged (3 hours after *Pto* inoculation) transcriptomes from leaf 1-2 (Col-0 and
658 *rSPL10*) and leaf 11 (Col-0) were compared. * indicates examples of leaf samples that
659 were collected for RNA-seq. Green: juvenile leaves; brown: adult leaves. **B**, an
660 expression profiling of DEGs identified in mock-treated adults against mock-treated
661 juvenile leaves. DEGs, differently expressed genes with LFC ≥ ±0.58 and padj ≤ 0.05.
662 LFC, log2 fold change of gene expression. Padj, adjusted p value. Color-codes in the
663 heatmap, blue is for down-regulated DEGs and red is for up-regulated DEGs.
664 Euclidean distance was used for calculating distance. Complete linkage was applied
665 to structure the hierarchical clustering. Expressing profiles of DEGs derived from
666 Adu-M/Juv-M are mapped in the first column of the map. The expressing profiles of
667 those DEGs in Adu-*P*/Juv-*P* are shown in the second column of the map. Genes that
668 were DEGs in both Adu-M/Juv-M and Adu-*P*/Juv-*P* are marked by the black bar on

669 the right. 38% indicates the percentage of those overlapping DEGs in Adu_{pto}. **C**, a
670 profile of *Pto*-triggered DEGs came from Juv-*P*/Juv-M and Adu-*P*/Adu-M.
671 Adult-specifically *Pto*-triggered DEGs (dark red), Juvenile-specifically triggered (light
672 brown), adult preferentially triggered (deep blue), and commonly triggered in both
673 adults and juveniles, i.e., shared (light grey) are marked by the first column of bars on
674 the right. The percentages (20.6%, 3.4%, 5.3%, 12.6%) and corresponding black bars
675 indicate the proportion of each DEG category that overlaps with Adu_{pto}. **D**,
676 representative GO terms enriched in DEGs of Adu_{nof}, DEGs triggered by *Pto* DC3000
677 in both adult and juvenile leaves (the Shared) and DEGs specifically triggered by *Pto*
678 in adult phase within the total Adu_{pto} (20.6%). Red and blue color blocks refer to GOs
679 enriched in up- and down-regulated DEGs, respectively. Only GO terms with FDR <
680 0.05 were deemed as enriched here. Fold enrichment was based on hypergeometric
681 tests within the range of the DEG set used for each GO analysis relative to
682 *Arabidopsis* genome. The analysis was done using the TAIR Gene ontology website
683 (geneontology.org). The same GO analysis and color-coding are used for Figure 4 C.
684
685 **Figure 4. *rSPL10* transcriptomes resembled that of adult leaves. A**, an
686 expression profiling of co-regulated DEGs by adult and *rSPL10* leaves at non-infected
687 state compared with juvenile leaves. *EDS1* and *PAD4* were identified as Adu/*r10*
688 co-upregulated DEGs under non-infected state, which are indicated in the heatmap
689 with arrows. **B**, expressing profiles of co-regulated DEGs by adult and *rSPL10* from
690 Adu-*P* or *r10-P* against Juv-*P*. For the clustered heatmaps in 4 A and B, blue
691 represents down-regulated DEGs and red is for up-regulated DEGs. Euclidean
692 distance was used for calculating distance in the partition around medoids (PAM)
693 clustering (k=4). **C**, GO enrichment of co-regulated adult and *r10 vs* juvenile DEGs in
694 non-infected and *Pto*-infection states.
695

696 **Figure 5, Salicylic acid (SA) biosynthesis and signaling were enhanced by**
697 **SPL10 in adult phase. A**, 672 up-regulated core SA markers were defined via
698 overlapping DEGs pools from Ding Y *et al.*, 2018 (dark circle) and Yang L *et al.*, 2017
699 (light circle). **B**, expression patterns of 527 detected (out of 672) up-regulated core SA
700 markers in adult and *r10* leaves, under non-infected and *Pto* infection states. Four
701 random pools of detected genes (450 genes per set) derived from each pair-wise
702 comparison exhibits here were chosen as negative controls. Up, upregulated. No, no
703 change. Down, downregulated. Y axis shows the negative logarithm transformed
704 adjusted p value, -log10(padj). X axis displays the value of Log2 fold change (LFC) of
705 gene expressions. M, mock. *P, Pto* DC3000. P < 0.0001 (Hypergeometric test, done
706 by GeneOverlap R package) was reproducibly output from each overlap between
707 core upregulated SA markers and Adu_{nof}, Adu_{pto}, $r10_{nof}$ and $r10_{pto}$ (SI Appendix,
708 information S6). The P values for 3 out of 4 random controls were not significant (SI
709 Appendix, information S6). **C**, endogenous SAG and free SA accumulation in juvenile,
710 *r10* and adult leaves at non-infected state. DW, dry weight. Repeats for the
711 experiment are shown in SI Appendix, Table S2. **D**, age-associated expression of four
712 SA markers in adult leaves from Col-0 and in comparable leaves of *spl2/10/11*.
713 Similar results were seen two times. **E**, the qPCR of the four SA marker genes in
714 juvenile, *r10* and adult leaves on sterile 1/2 MS plates. Similar results were seen three
715 times. **F**, overrepresentation of EDS1-PAD4 core regulon (EP core) in Adu/$r10_{nof}$ and
716 Adu/$r10_{pto}$. The EP core markers were defined in Cui *et al.,* 2017 (46). 127/155 of the
717 EP core markers were detected in this work. Randomly selected 127 genes from our
718 RNA-seq dataset were used as controls.
719
720 **Figure 6, *PAD4* was a direct target of SPL10. A**, Overlap between Adu/$r10_{nof}$
721 co-regulated genes and potential SPL10 targets defined according to ChIP-seq data
722 from *Ye et al*. (upper panel). A motif discovery and enrichment analysis of the 203
723 Adu/$r10_{nof}$ co-upregulated DEGs (lower panel). **B**, SPL10 bound to a

724 GTAC-containing motif upstream of *PAD4*. qPCR following chromatin
725 immunoprecipitation of *rSPL10*-YFP for motifs (M1 and M2) and negative control sites
726 (nc1 and nc2) are at least 600 bp away from M1 and M2 at the *PAD4* genomic region.
727 Three primer sets (p1-p3) were used to amplify the M1 site. Relative locations of ChIP
728 peaks (dark grey) derived from *Ye et al*, primers (arrow pairs) and the tested sites
729 (color blocks) were indicated in the schematic diagram. The student t test was
730 performed to compare and indicate the significance of difference between the sites. **C**,
731 qPCR of *PAD4* transcripts level in juvenile (Juv) and adult (Adu) leaves of Col-0 and
732 *spl2/10/11*. The student t test, ns, not significant, *, $p < 0.05$, **, $p < 0.01$.
733
734 **Figure 7, SA biosynthesis and signaling components were required for the**
735 **SPL10 regulated ARR_{VPC}. A**, a comparison of *Pto* DC3000 growth between the
736 juvenile and adult leaves (ARR phenotype) of Col-0, *sid2-1* and *npr1-1*. **B**,
737 developmental phenotype (top) and the bacterial growth (bottom) in 4-week-old
738 leaves 1 and 2 from Col-0, *sid2-1*, *MIM156* and *MIM156/sid2-1*. **C**, developmental
739 phenotype of 4-week-old Col-0, *eds1.2, r10* and *r10 /eds1.2*. Note the similar leaf
740 shape between *r10* and *r10*/*eds1.2;* (bottom panel) bacterial multiplication in leaves 1
741 and 2 derived from Col-0, *eds1.2*, *r10* and *rSPL10/eds1.2*. Arrows indicate leaves 1-2.
742 **D**, the ARR phenotyping of *eds1.2* and *pad4-1* infected with *Pto* DC3000. Emmeans
743 package in R was used for statistical analysis in 7 A and D. The student t test was
744 used for statistical analysis in 7 B-C, and each genotype was compared with Col-0
745 wild type, ns, not significant, *, $p < 0.05$, **, $p < 0.01$.
746
747 **Figure S1, Ontogenic change of SA response and sampling approach for**
748 **examining ARR_{vpc}. A,** ontogenic-associated promoter activities of pro*PR2*::GUS in
749 an uninfected plant. Note the high activity in fully expanded juvenile leaves (1-7) and
750 low in young adult leaves (12-13). The indicated leaf numbers were based on the
751 order of the leaves on shoot. **B**, the incremental expression of *PR2* gene spanning the

752 expansion of juvenile and adult leaves. I, premature leaves. II, intermediate premature
753 leaves. III, mature leaves. **C**, An outline of the ontogenic maturation of a juvenile leaf
754 and an adult leaf. The boxed region indicates distinct ontogenic age of juvenile and
755 adult leaves from the same plant; asteroids indicate juvenile and adult leaves of the
756 same ontogenic age. **D,** The quantified leaf expansion rate in juvenile and adult
757 leaves. Leaf areas were quantified and normalized through Fiji software. **E**, a cartoon
758 depiction of shoot development and leaf maturation that are concurrent during the
759 vegetative phase change.
760
761 **Figure S2. Developmental phenotypes of *rSPLs* and *spl* mutants. A and D**,
762 arrows indicate leaf 1-2 of juvenile Col-0 and *rSPLs*. **B-C**, arrows indicate
763 representative adult leaves of Col-0 and *spl* mutants.
764
765 **Figure S3. Quality control of RNA-seq datasets and Venn diagrams of adult *vs***
766 **juvenile DEGs. A**, principal component analysis showed that the effect of age and
767 genotype likely explained 52% variance of the samples, and *Pto* infection effect likely
768 explained 17% variance of the samples. **B**, the sample-to-sample distance matrix
769 showed that biological replicates (Mock1-3 and *Pto*1-3) were well correlated (in close
770 distance) within per genotype per treatment. The column names of the matrix are in
771 the same order as the row names--from the "Adu-Mock1" (the first on the left) to the
772 *"r10-Pto3*" (the first on the right). **C**, venn diagrams of Adu-DEGs generated from the
773 indicated pair-wise comparisons. Color-coding of numbers, adult-specifically
774 *Pto*-triggered DEGs (red), Juvenile-specifically triggered (brown), commonly triggered
775 in both adults and juveniles, i.e., shared (grey), and overlap DEGs between Adu_{nof}
776 and Adu_{pto} (black). Green numbers indicate the 20.1% synergistic DEGs that
777 mentioned in the main text. Blue numbers refer to DEGs that were Adu_{nof} but not
778 Adu_{pto}. Adult preferentially *Pto*-triggered DEGs are listed in SI Appendix Table S3.
779

780 **Figure S4. Expression of *SPL3* and *SPL10* in *MIM156/sid2-1* and *r10/eds1.2*.**
781 A, *SPL3* was used as an indicator of *MIM156* function. No difference was observed in
782 *MIM156* and *MIM156/sid2-1.* B, *SPL10* was expressed at comparable level in *rSPL10*
783 and *rSPL10/eds1.2.* Student t test, ns, not significant, *, $p < 0.05$, **, $p < 0.01$.
784
785 **Figure S5. A table of enriched SPL-binding motifs within the upregulated 203**
786 **and plant phenotype of *proSPL10::rSPL10-YFP*. A. Adu/*r10*$_{nof}$ co-regulon**.
787 Frequency-based DNA logos are shown for each enriched motif. The analysis was
788 performed in the simple enrichment analysis-MEME Suite. Details were described in
789 the method section. **B.** plant phenotype of proSPL10::rSPL10-YFP. Note the
790 elongated leaves 1 and 2 in the transgenic plant.
791
792 **Figure S6. A model of miR156-SPL10 regulated age-related resistance during**
793 **the vegetative phase change.** In brief, miR156 suppressed the resistance in juvenile
794 phase through inhibiting SPL10. The increased expression of *SPL10* followed by the
795 decline of miR156 level gives rise to a high immune output in adult phase. That is
796 achieved via promoting the expression of *PAD4* as well as enhancing expressions of
797 components in SA biosynthesis and signaling pathways.
798
799
800
801
802
803
804
805
806
807

808

809

810 **Reference**

811 1. R. Solana, G. Pawelec, R. Tarazona, Aging and innate immunity. *Immunity* **24**,
812 491-494 (2006).
813 2. R. Solana *et al.*, Innate immunosenescence: effect of aging on cells and
814 receptors of the innate immune system in humans. *Semin Immunol* **24**,
815 331-341 (2012).
816 3. M. P. Develey-Rivière, E. Galiana, Resistance to pathogens and host
817 developmental stage: a multifaceted relationship within the plant kingdom.
818 *New Phytologist* **175**, 405-416 (2007).
819 4. L. Hu, L. Yang, Time to fight: Molecular mechanisms of age-related resistance.
820 *Phytopathology* **109**, 1500-1508 (2019).
821 5. Y. Zou *et al.*, Transcriptional regulation of the immune receptor FLS2 controls
822 the ontogeny of plant innate immunity. *The Plant Cell* **30**, 2779-2794 (2018).
823 6. M. Chandler, W. Tracy, Vegetative phase change among sweet corn (Zea
824 mays L.) hybrids varying for reaction to common rust (Puccinia sorghi Schw.).
825 *Plant breeding* **126**, 569-573 (2007).
826 7. C. Rusterucci *et al.*, Age-related resistance to Pseudomonas syringae pv.
827 tomato is associated with the transition to flowering in Arabidopsis and is
828 effective against Peronospora parasitica. *Physiological and molecular plant*
829 *pathology* **66**, 222-231 (2005).
830 8. S. Glander *et al.*, Assortment of flowering time and immunity alleles in
831 natural Arabidopsis thaliana populations suggests immunity and vegetative
832 lifespan strategies coevolve. *Genome biology and evolution* **10**, 2278-2291
833 (2018).
834 9. S. R. Paludan, T. Pradeu, S. L. Masters, T. H. Mogensen, Constitutive immune
835 mechanisms: mediators of host defence and immune regulation. *Nat Rev*
836 *Immunol* **21**, 137-150 (2021).
837 10. S. Panter, D. A. Jones, Age-related resistance to plant pathogens. (2002).
838 11. R. S. Poethig, "Vegetative phase change and shoot maturation in plants" in
839 Current topics in developmental biology. (Elsevier, 2013), vol. 105, pp.
840 125-152.
841 12. R. A. Brink, Phase change in higher plants and somatic cell heredity. *The*
842 *Quarterly Review of Biology* **37**, 1-22 (1962).
843 13. R. S. Poethig, Phase change and the regulation of shoot morphogenesis in
844 plants. *Science* **250**, 923-930 (1990).
845 14. S. A. Alzohairy, R. Hammerschmidt, M. K. Hausbeck, Changes in winter squash
846 fruit exocarp structure associated with age-related resistance to
847 Phytophthora capsici. *Phytopathology* **110**, 447-455 (2020).
848 15. P. Carella, D. C. Wilson, R. K. Cameron, Some things get better with age:
849 differences in salicylic acid accumulation and defense signaling in young and
850 mature Arabidopsis. *Frontiers in plant science* **5**, 775 (2015).
851 16. J.-W. Wang *et al.*, miRNA control of vegetative phase change in trees. *PLoS*
852 *Genet* **7**, e1002012 (2011).

853 17. R. P. Birkenbihl, G. Jach, H. Saedler, P. Huijser, Functional dissection of the
854 plant-specific SBP-domain: overlap of the DNA-binding and nuclear
855 localization domains. *Journal of molecular biology* **352**, 585-596 (2005).
856 18. X. Liang, T. J. Nazarenus, J. M. Stone, Identification of a consensus
857 DNA-binding site for the Arabidopsis thaliana SBP domain transcription factor,
858 AtSPL14, and binding kinetics by surface plasmon resonance. *Biochemistry* **47**,
859 3645-3653 (2008).
860 19. M. W. Rhoades *et al.*, Prediction of plant microRNA targets. *Cell* **110**, 513-520
861 (2002).
862 20. G. Wu, R. S. Poethig, Temporal regulation of shoot development in
863 Arabidopsis thaliana by miR156 and its target SPL3. *Development* **133**,
864 3539-3547 (2006).
865 21. G. Wu *et al.*, The sequential action of miR156 and miR172 regulates
866 developmental timing in Arabidopsis. *Cell* **138**, 750-759 (2009).
867 22. M. Gandikota *et al.*, The miRNA156/157 recognition element in the 3' UTR of
868 the Arabidopsis SBP box gene SPL3 prevents early flowering by translational
869 inhibition in seedlings. *The Plant Journal* **49**, 683-693 (2007).
870 23. H. Wang, H. Wang, The miR156/SPL module, a regulatory hub and versatile
871 toolbox, gears up crops for enhanced agronomic traits. *Molecular plant* **8**,
872 677-688 (2015).
873 24. M. Xu *et al.*, Developmental functions of miR156-regulated SQUAMOSA
874 PROMOTER BINDING PROTEIN-LIKE (SPL) genes in Arabidopsis thaliana. *PLoS*
875 *genetics* **12**, e1006263 (2016).
876 25. B.-B. Ye *et al.*, AP2/ERF transcription factors integrate age and wound signals
877 for root regeneration. *The Plant Cell* **32**, 226-241 (2020).
878 26. G. Cardon *et al.*, Molecular characterisation of the Arabidopsis SBP-box genes.
879 *Gene* **237**, 91-104 (1999).
880 27. T. Sun *et al.*, SQUINT Positively Regulates Resistance to the Pathogen Botrytis
881 cinerea via miR156–SPL9 Module in Arabidopsis. *Plant and Cell Physiology* **0**
882 (2022).
883 28. H. Yin *et al.*, miR156/SPL9 Regulates Reactive Oxygen Species Accumulation
884 and Immune Response in Arabidopsis thaliana. *Phytopathology* **109**,
885 PHYTO-08-18-0306-R (2019).
886 29. M. L. Berens *et al.*, Balancing trade-offs between biotic and abiotic stress
887 responses through leaf age-dependent variation in stress hormone cross-talk.
888 *Proc Natl Acad Sci U S A* **116**, 2364-2373 (2019).
889 30. A. Kanojia *et al.*, Developmentally controlled changes during Arabidopsis leaf
890 development indicate causes for loss of stress tolerance with age. *Journal of*
891 *experimental botany* **71**, 6340-6354 (2020).
892 31. B. N. Mansfeld, M. Colle, Y. Kang, A. D. Jones, R. Grumet, Transcriptomic and
893 metabolomic analyses of cucumber fruit peels reveal a developmental
894 increase in terpenoid glycosides associated with age-related resistance to
895 Phytophthora capsici. *Horticulture research* **4** (2017).
896 32. B. N. Mansfeld, M. Colle, C. Zhang, Y.-C. Lin, R. Grumet, Developmentally
897 regulated activation of defense allows for rapid inhibition of infection in
898 age-related resistance to Phytophthora capsici in cucumber fruit. *BMC*
899 *genomics* **21**, 1-25 (2020).

900 33. D. C. Wilson, P. Carella, M. Isaacs, R. K. Cameron, The floral transition is not
901 the developmental switch that confers competence for the Arabidopsis
902 age-related resistance response to Pseudomonas syringae pv. tomato. *Plant*
903 *molecular biology* **83**, 235-246 (2013).
904 34. J. L. Carviel *et al.*, Forward and reverse genetics to identify genes involved in
905 the age-related resistance response in Arabidopsis thaliana. *Molecular plant*
906 *pathology* **10**, 621-634 (2009).
907 35. J. He *et al.*, Threshold-dependent repression of SPL gene expression by
908 miR156/miR157 controls vegetative phase change in Arabidopsis thaliana.
909 *PLoS Genet* **14**, e1007337 (2018).
910 36. J. M. Franco-Zorrilla *et al.*, Target mimicry provides a new mechanism for
911 regulation of microRNA activity. *Nature genetics* **39**, 1033 (2007).
912 37. A.-Y. Guo *et al.*, Genome-wide identification and evolutionary analysis of the
913 plant specific SBP-box transcription factor family. *Gene* **418**, 1-8 (2008).
914 38. M. S. Padmanabhan *et al.*, Novel positive regulatory role for the SPL6
915 transcription factor in the N TIR-NB-LRR receptor-mediated plant innate
916 immunity. *PLoS pathogens* **9**, e1003235 (2013).
917 39. A. Yamaguchi *et al.*, The microRNA-regulated SBP-Box transcription factor
918 SPL3 is a direct upstream activator of LEAFY, FRUITFULL, and APETALA1.
919 *Developmental cell* **17**, 268-278 (2009).
920 40. P. Ding *et al.*, Chromatin accessibility landscapes activated by cell-surface and
921 intracellular immune receptors. *Journal of Experimental Botany* **72**,
922 7927-7941 (2021).
923 41. A. Telfer, K. M. Bollman, R. S. Poethig, Phase change and the regulation of
924 trichome distribution in Arabidopsis thaliana. *Development* **124**, 645-654
925 (1997).
926 42. J. S. Thaler, P. T. Humphrey, N. K. Whiteman, Evolution of jasmonate and
927 salicylate signal crosstalk. *Trends in plant science* **17**, 260-270 (2012).
928 43. K. Ando, K. M. Carr, M. Colle, B. N. Mansfeld, R. Grumet, Exocarp Properties
929 and Transcriptomic Analysis of Cucumber (Cucumis sativus) Fruit Expressing
930 Age-Related Resistance to Phytophthora capsici. *PLoS One* **10**, e0142133
931 (2015).
932 44. L. Yang *et al.*, Pseudomonas syringae Type III Effector HopBB1 Promotes Host
933 Transcriptional Repressor Degradation to Regulate Phytohormone Responses
934 and Virulence. *Cell Host Microbe* **21**, 156-168 (2017).
935 45. Y. Ding *et al.*, Opposite roles of salicylic acid receptors NPR1 and NPR3/NPR4
936 in transcriptional regulation of plant immunity. *Cell* **173**, 1454-1467. e1415
937 (2018).
938 46. H. Cui *et al.*, A core function of EDS1 with PAD4 is to protect the salicylic acid
939 defense sector in Arabidopsis immunity. *New Phytologist* **213**, 1802-1817
940 (2017).
941 47. R. C. O'Malley *et al.*, Cistrome and epicistrome features shape the regulatory
942 DNA landscape. *Cell* **165**, 1280-1292 (2016).
943 48. M. Liu *et al.*, Inducible overexpression of Ideal Plant Architecture1 improves
944 both yield and disease resistance in rice. *Nature plants*, 1 (2019).
945 49. J. Wang *et al.*, A single transcription factor promotes both yield and immunity
946 in rice. *Science* **361**, 1026-1028 (2018).

947 50. Y. Deng *et al.*, A role for small RNA in regulating innate immunity during plant
948 growth. *PLoS pathogens* **14**, e1006756 (2018).
949 51. N. Yalpani, V. Shulaev, I. Raskin, Endogenous salicylic acid levels correlate
950 with accumulation of pathogenesis-related proteins and virus resistance in
951 tobacco. *Phytopathology* **83**, 702-708 (1993).
952 52. D. C. Wilson, C. J. Kempthorne, P. Carella, D. K. Liscombe, R. K. Cameron,
953 Age-Related Resistance in Arabidopsis thaliana Involves the MADS-Domain
954 Transcription Factor SHORT VEGETATIVE PHASE and Direct Action of Salicylic
955 Acid on Pseudomonas syringae. *Mol Plant Microbe Interact* **30**, 919-929
956 (2017).
957 53. D. C. Wilson, P. Carella, M. Isaacs, R. K. Cameron, The floral transition is not
958 the developmental switch that confers competence for the Arabidopsis
959 age-related resistance response to Pseudomonas syringae pv. tomato. *Plant*
960 *Mol Biol* **83**, 235-246 (2013).
961 54. J. V. Kus, K. Zaton, R. Sarkar, R. K. Cameron, Age-related resistance in
962 Arabidopsis is a developmentally regulated defense response to
963 Pseudomonas syringae. *The Plant Cell* **14**, 479-490 (2002).
964 55. T. Fukao, B. E. Barrera-Figueroa, P. Juntawong, J. M. Pena-Castro,
965 Submergence and Waterlogging Stress in Plants: A Review Highlighting
966 Research Opportunities and Understudied Aspects. *Front Plant Sci* **10**, 340
967 (2019).
968 56. J. D. Jones, R. E. Vance, J. L. Dangl, Intracellular innate immune surveillance
969 devices in plants and animals. *Science* **354**, aaf6395 (2016).
970 57. Y. Rossez, E. B. Wolfson, A. Holmes, D. L. Gally, N. J. Holden, Bacterial flagella:
971 twist and stick, or dodge across the kingdoms. *PLoS pathogens* **11**, e1004483
972 (2015).
973 58. B. J. Reinhart *et al.*, The 21-nucleotide let-7 RNA regulates developmental
974 timing in Caenorhabditis elegans. *nature* **403**, 901-906 (2000).
975 59. A. L. Abbott *et al.*, The let-7 MicroRNA family members mir-48, mir-84, and
976 mir-241 function together to regulate developmental timing in
977 Caenorhabditis elegans. *Developmental cell* **9**, 403-414 (2005).
978 60. Z. Ren, V. R. Ambros, Caenorhabditis elegans microRNAs of the let-7 family
979 act in innate immune response circuits and confer robust developmental
980 timing against pathogen stress. *Proceedings of the National Academy of*
981 *Sciences* **112**, E2366-E2375 (2015).
982 61. D. Kim, J. M. Paggi, C. Park, C. Bennett, S. L. Salzberg, Graph-based genome
983 alignment and genotyping with HISAT2 and HISAT-genotype. *Nat Biotechnol*
984 **37**, 907-915 (2019).
985 62. P. Lamesch *et al.*, The Arabidopsis Information Resource (TAIR): improved
986 gene annotation and new tools. *Nucleic Acids Res* **40**, D1202-1210 (2012).
987 63. D. Swarbreck *et al.*, The Arabidopsis Information Resource (TAIR): gene
988 structure and function annotation. *Nucleic Acids Res* **36**, D1009-1014 (2008).
989 64. M. Pertea, D. Kim, G. M. Pertea, J. T. Leek, S. L. Salzberg, Transcript-level
990 expression analysis of RNA-seq experiments with HISAT, StringTie and
991 Ballgown. *Nat Protoc* **11**, 1650-1667 (2016).
992 65. M. I. Love, W. Huber, S. Anders, Moderated estimation of fold change and
993 dispersion for RNA-seq data with DESeq2. *Genome Biol* **15**, 550 (2014).

994 66. K. Dolinski *et al.*, Gene ontology: tool for the unification of biology. The Gene
995 Ontology Consortium. *Nat Genet* **25**, 2529Attri (2000).
996 67. Anonymous, The Gene Ontology resource: enriching a GOld mine. *Nucleic*
997 *acids research* **49**, D325-D334 (2021).
998 68. T. Tian *et al.*, agriGO v2.0: a GO analysis toolkit for the agricultural
999 community, 2017 update. *Nucleic Acids Res* **45**, W122-W129 (2017).
1000 69. Z. Gu, R. Eils, M. Schlesner, Complex heatmaps reveal patterns and
1001 correlations in multidimensional genomic data. *Bioinformatics* **32**, 2847-2849
1002 (2016).
1003 70. L. Brand *et al.*, A versatile and reliable two-component system for
1004 tissue-specific gene induction in Arabidopsis. *Plant Physiol* **141**, 1194-1204
1005 (2006).
1006 71. W. A. Ricci, L. Levin, X. Zhang, "Genome-Wide Profiling of Histone
1007 Modifications with ChIP-Seq" in Cereal Genomics. (Springer, 2020), pp.
1008 101-117.
1009 72. N. Yamaguchi *et al.*, PROTOCOLS: Chromatin immunoprecipitation from
1010 Arabidopsis tissues. *The Arabidopsis book/American Society of Plant*
1011 *Biologists* **12** (2014).
1012 73. X. Lin, L. Tirichine, C. Bowler, Protocol: Chromatin immunoprecipitation (ChIP)
1013 methodology to investigate histone modifications in two model diatom
1014 species. *Plant methods* **8**, 1-9 (2012).
1015

Figure 1

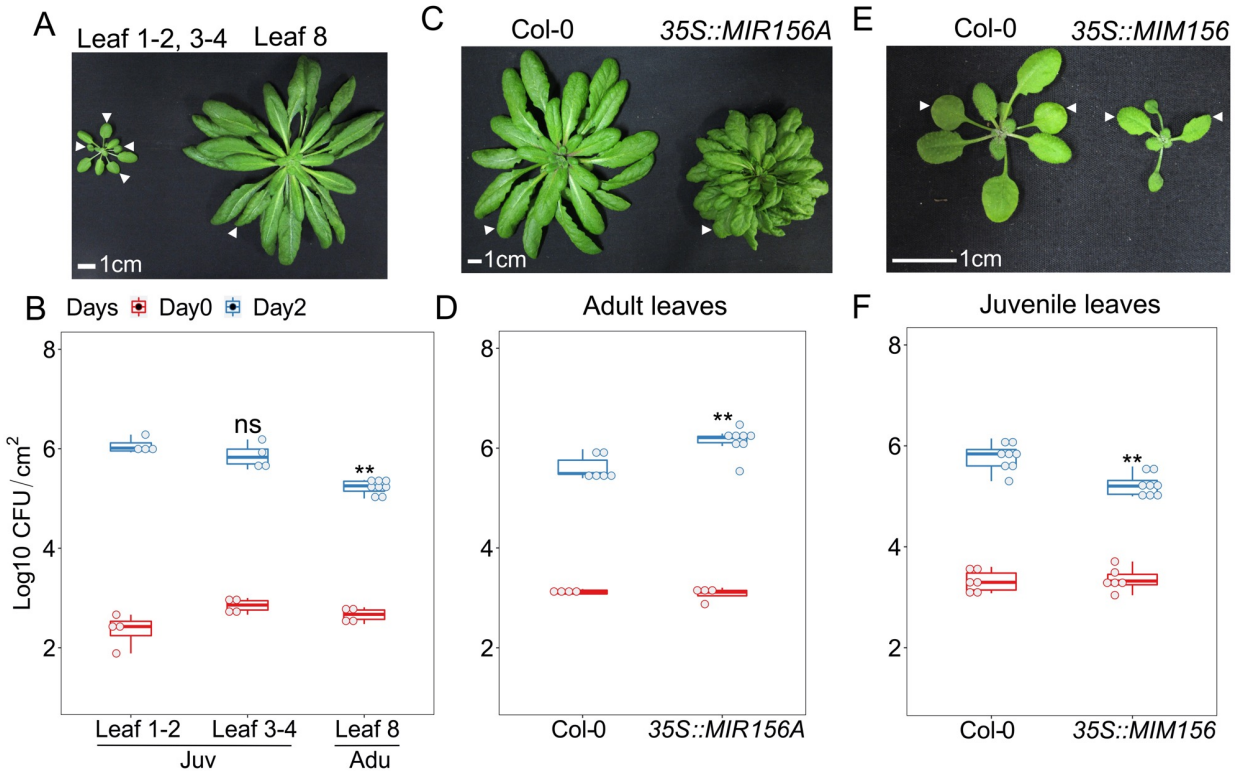
A
Leaf 1-2, 3-4
Leaf 8
1cm
C
Col-0
35S::MIR156A
1cm
E
Col-0
35S::MIM156
1cm
B
Days
Day0
Day2
Log10 CFU / cm2
ns
**
Leaf 1-2
Leaf 3-4
Leaf 8
Juv
Adu
D
Adult leaves
**
Col-0
35S::MIR156A
F
Juvenile leaves
**
Col-0
35S::MIM156

Figure 2

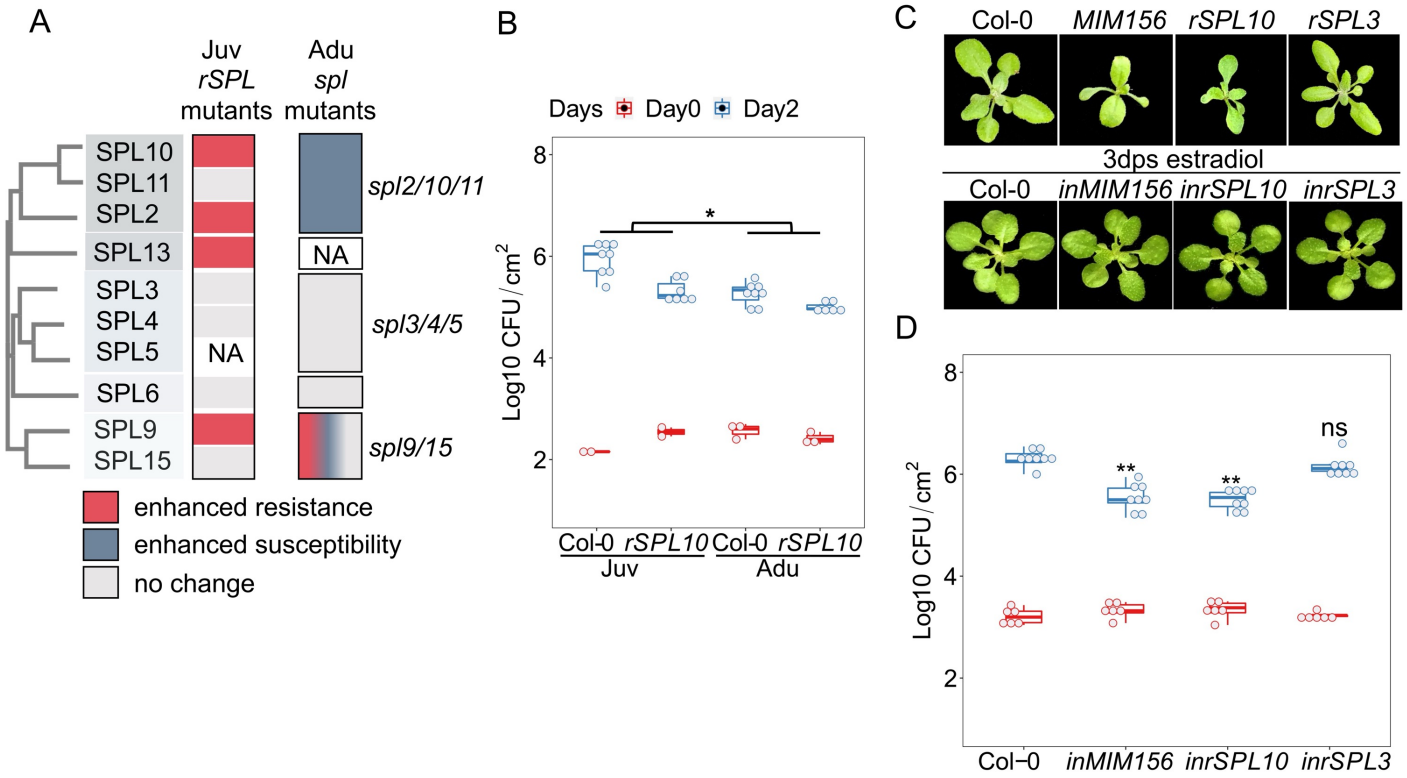
A
Juv
rSPL
mutants
Adu
spl
mutants
SPL10
SPL11
SPL2
SPL13
SPL3
SPL4
SPL5
SPL6
SPL9
SPL15
NA
spl2/10/11
NA
spl3/4/5
spl9/15
enhanced resistance
enhanced susceptibility
no change
B
Days
Day0
Day2
Log10 CFU / cm2
8
6
4
2
*
Col-0
rSPL10
Col-0
rSPL10
Juv
Adu
C
Col-0
MIM156
rSPL10
rSPL3
3dps estradiol
Col-0
inMIM156
inrSPL10
inrSPL3
D
Log10 CFU / cm2
8
6
4
2
**
**
ns
Col-0
inMIM156
inrSPL10
inrSPL3

Figure 3

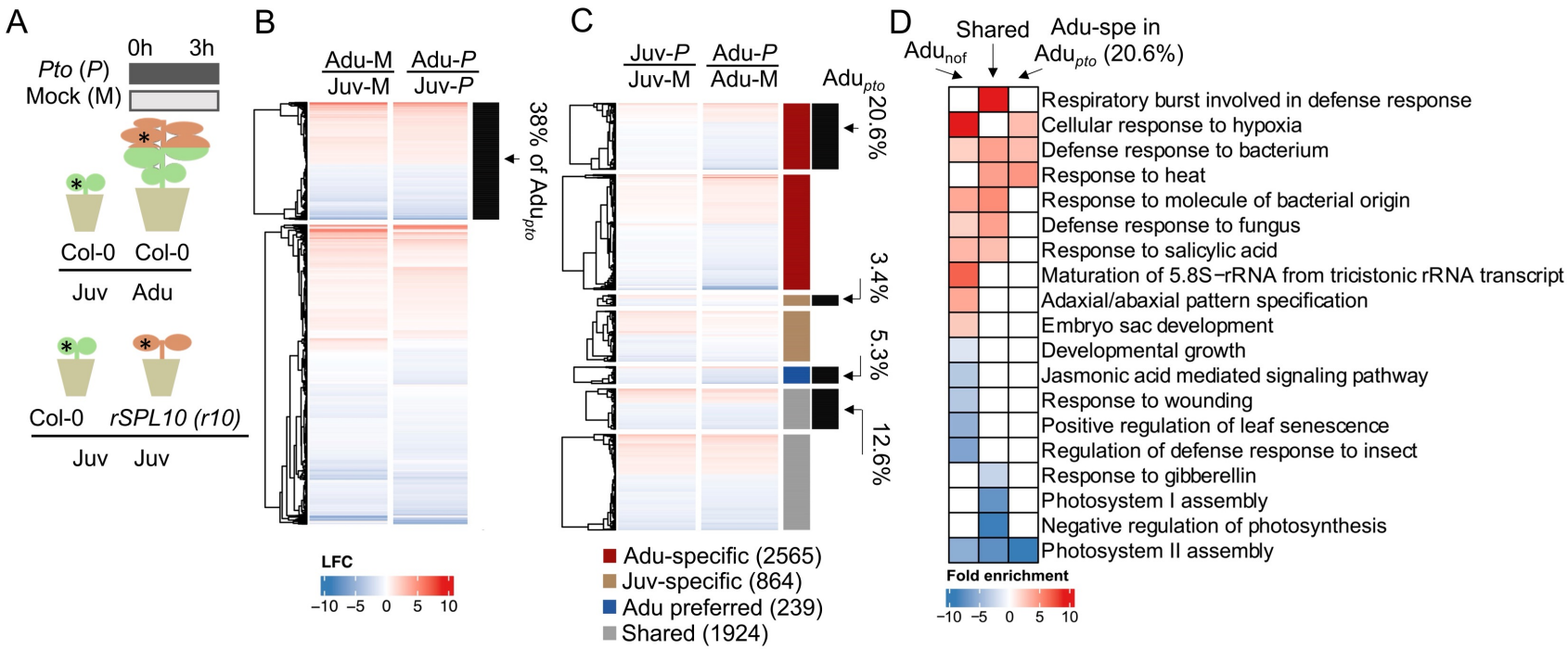
A
0h
3h
Pto (P)
Mock (M)
Col-0
Col-0
Juv
Adu
Col-0
rSPL10 (r10)
Juv
Juv
B
Adu-M / Juv-M
Adu-P / Juv-P
38% of Adupto
LFC
−10 −5 0 5 10
C
Juv-P / Juv-M
Adu-P / Adu-M
Adupto
20.6%
3.4%
5.3%
12.6%
Adu-specific (2565)
Juv-specific (864)
Adu preferred (239)
Shared (1924)
D
Adunof
Shared
Adu-spe in Adupto (20.6%)
Respiratory burst involved in defense response
Cellular response to hypoxia
Defense response to bacterium
Response to heat
Response to molecule of bacterial origin
Defense response to fungus
Response to salicylic acid
Maturation of 5.8S−rRNA from tricistonic rRNA transcript
Adaxial/abaxial pattern specification
Embryo sac development
Developmental growth
Jasmonic acid mediated signaling pathway
Response to wounding
Positive regulation of leaf senescence
Regulation of defense response to insect
Response to gibberellin
Photosystem I assembly
Negative regulation of photosynthesis
Photosystem II assembly
Fold enrichment
−10 −5 0 5 10

Figure 4

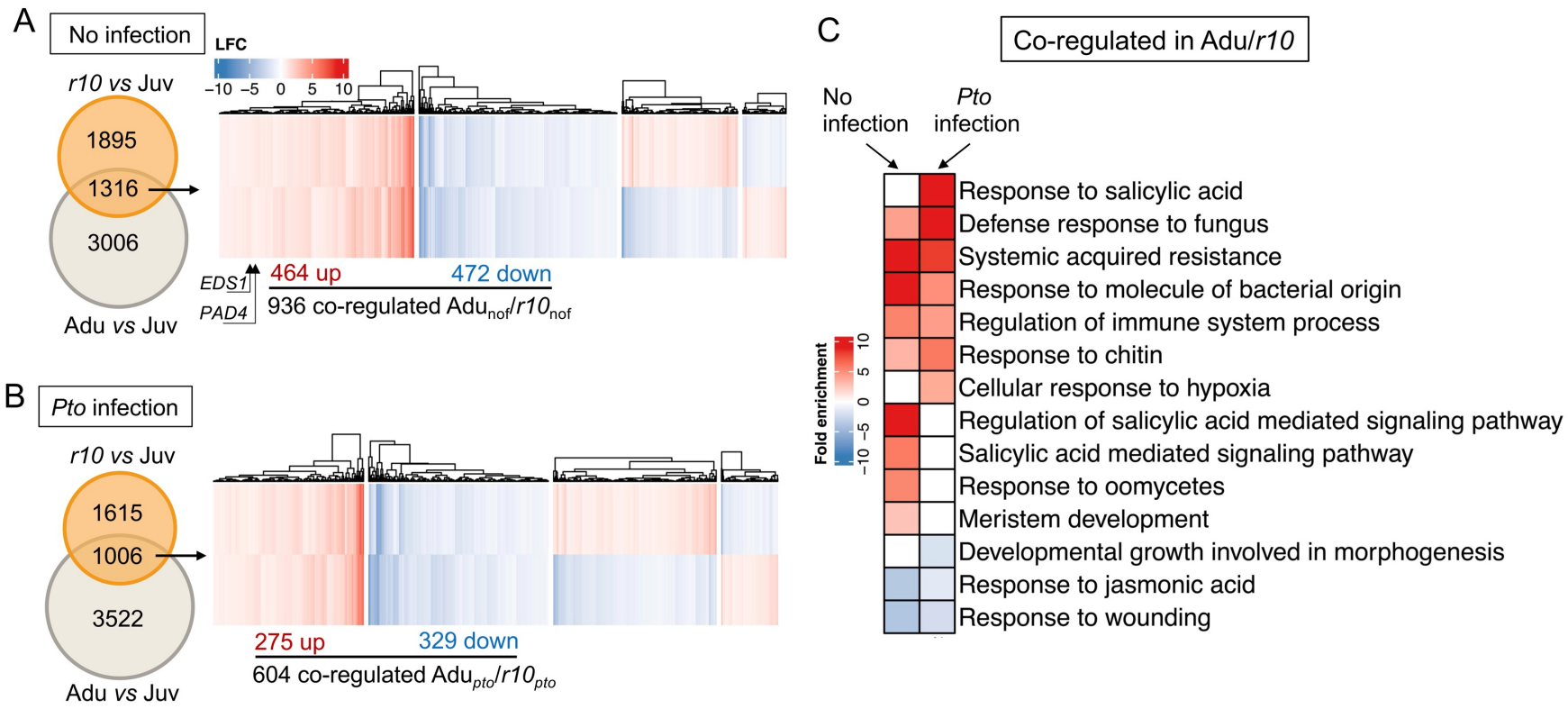
A
No infection
r10 vs Juv
1895
1316
3006
Adu vs Juv
LFC
−10 −5 0 5 10
EDS1
PAD4
464 up
472 down
936 co-regulated Adu$_{nof}$/r10$_{nof}$
B
Pto infection
r10 vs Juv
1615
1006
3522
Adu vs Juv
275 up
329 down
604 co-regulated Adu$_{pto}$/r10$_{pto}$
C
Co-regulated in Adu/r10
No infection
Pto infection
Fold enrichment
−10 −5 0 5 10
Response to salicylic acid
Defense response to fungus
Systemic acquired resistance
Response to molecule of bacterial origin
Regulation of immune system process
Response to chitin
Cellular response to hypoxia
Regulation of salicylic acid mediated signaling pathway
Salicylic acid mediated signaling pathway
Response to oomycetes
Meristem development
Developmental growth involved in morphogenesis
Response to jasmonic acid
Response to wounding

Figure 5

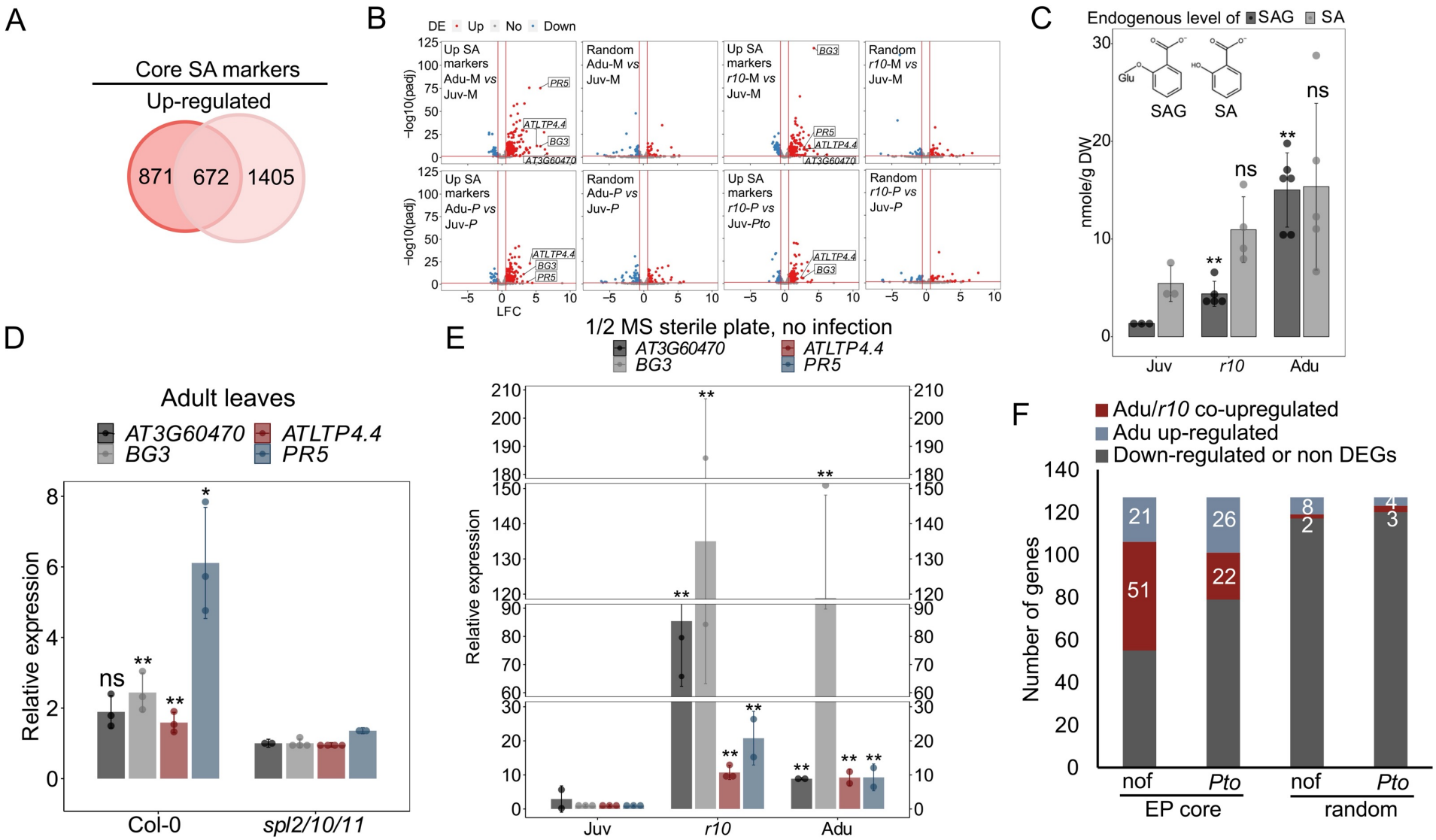
A
Core SA markers
Up-regulated
871
672
1405
B
DE Up No Down
Up SA markers Adu-M vs Juv-M
Random Adu-M vs Juv-M
Up SA markers r10-M vs Juv-M
Random r10-M vs Juv-M
Up SA markers Adu-P vs Juv-P
Random Adu-P vs Juv-P
Up SA markers r10-P vs Juv-Pto
Random r10-P vs Juv-P
PR5
ATLTP4.4
BG3
AT3G60470
−log10(padj)
LFC
C
Endogenous level of SAG SA
Glu
SAG
SA
nmole/g DW
ns
**
Juv
r10
Adu
D
Adult leaves
AT3G60470
BG3
ATLTP4.4
PR5
Relative expression
ns
**
*
Col-0
spl2/10/11
E
1/2 MS sterile plate, no infection
AT3G60470
BG3
ATLTP4.4
PR5
Relative expression
**
Juv
r10
Adu
F
Adu/r10 co-upregulated
Adu up-regulated
Down-regulated or non DEGs
Number of genes
21
51
26
22
8
2
4
3
nof
Pto
EP core
random

Figure 6

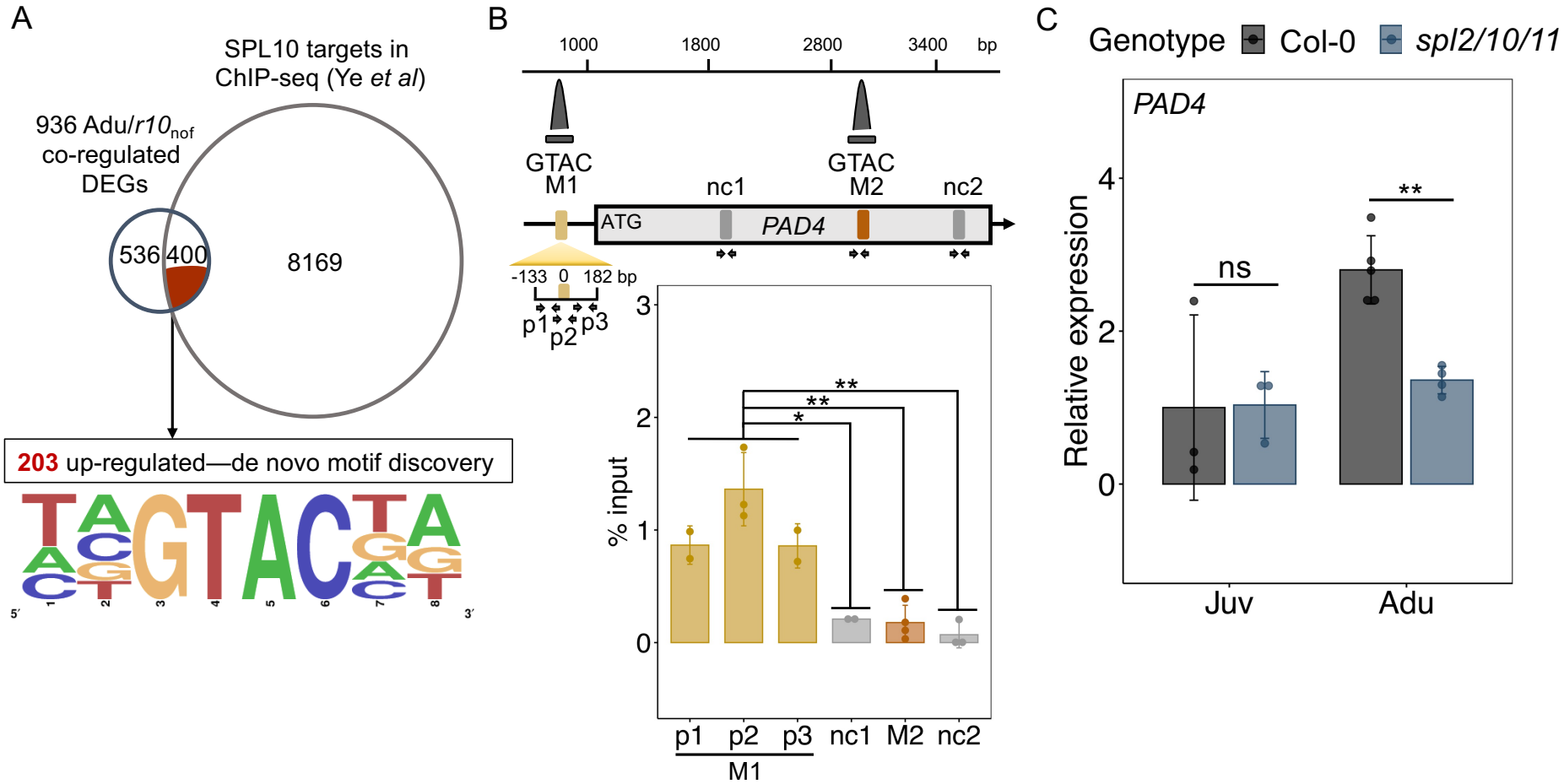
A
SPL10 targets in
ChIP-seq (Ye et al)
936 Adu/r10nof
co-regulated
DEGs
536
400
8169
203 up-regulated—de novo motif discovery
B
1000
1800
2800
3400
bp
GTAC
M1
GTAC
M2
nc1
nc2
ATG
PAD4
-133
0
182 bp
p1
p2
p3
% input
p1
p2
p3
nc1
M2
nc2
M1
C
Genotype
Col-0
spl2/10/11
PAD4
Relative expression
ns
Juv
Adu

Figure 7

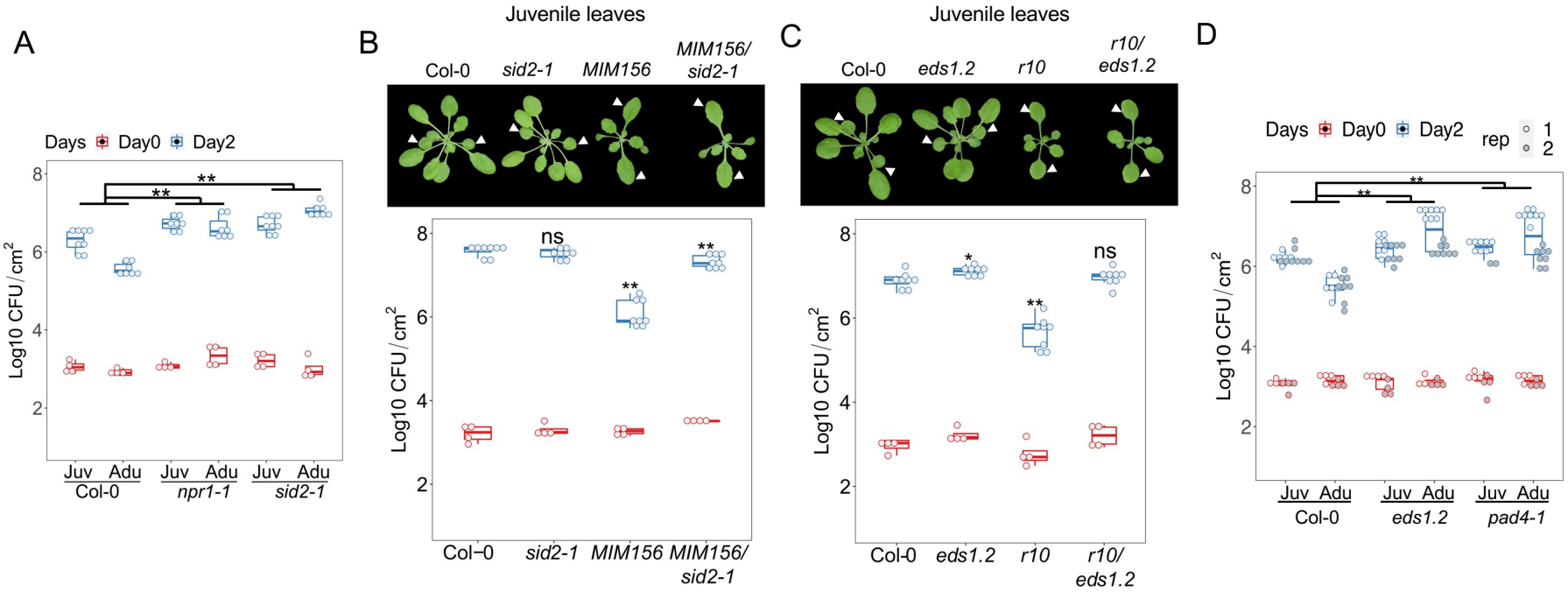
A
Days Day0 Day2
Log10 CFU/cm2
Juv Adu Juv Adu Juv Adu
Col-0 npr1-1 sid2-1
B
Juvenile leaves
Col-0 sid2-1 MIM156 MIM156/ sid2-1
ns
Col-0 sid2-1 MIM156 MIM156/ sid2-1
C
Juvenile leaves
Col-0 eds1.2 r10 r10/ eds1.2
ns
Col-0 eds1.2 r10 r10/ eds1.2
D
Days Day0 Day2
rep 1 2
Juv Adu Juv Adu Juv Adu
Col-0 eds1.2 pad4-1

Figure S1

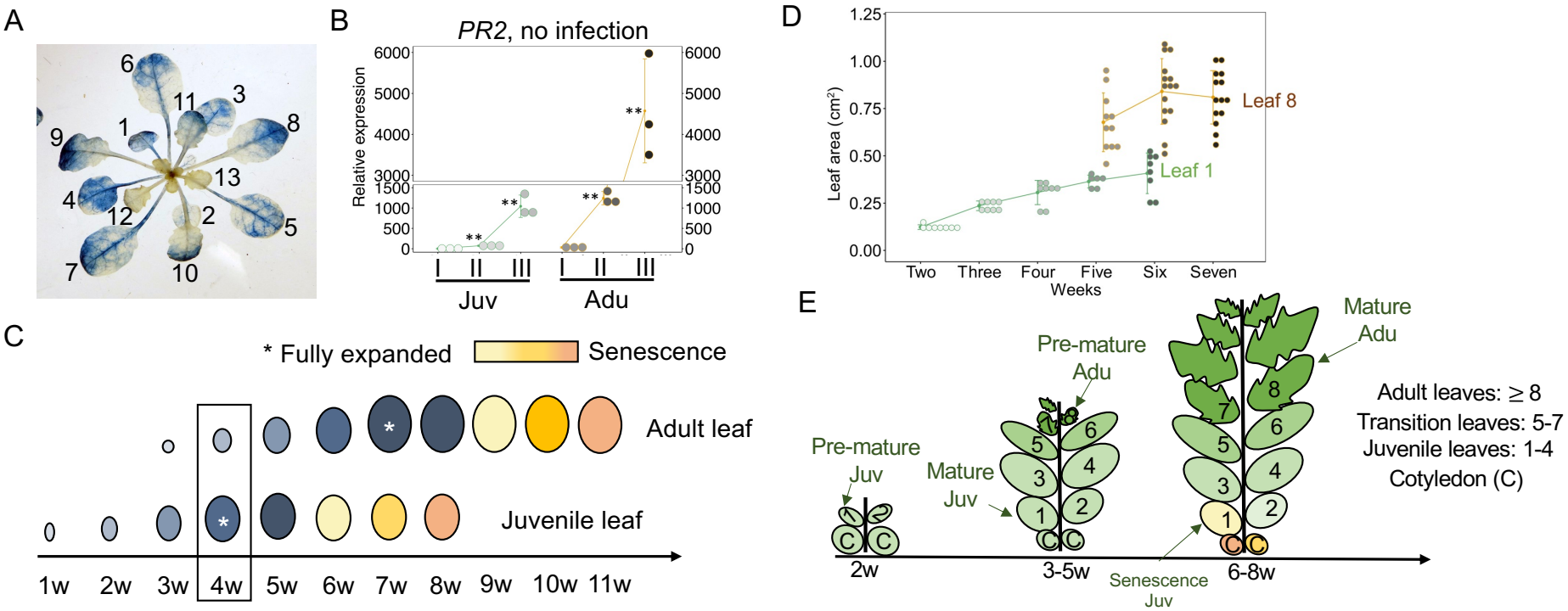
A
6
11
3
9
1
8
13
4
12
2
5
7
10
B
PR2, no infection
Relative expression
6000
5000
4000
3000
1500
1000
500
0
**
I II III
Juv
Adu
C
* Fully expanded
Senescence
Adult leaf
Juvenile leaf
1w 2w 3w 4w 5w 6w 7w 8w 9w 10w 11w
D
Leaf area (cm²)
1.25
1.00
0.75
0.50
0.25
0.00
Leaf 8
Leaf 1
Two Three Four Five Six Seven
Weeks
E
Mature Adu
Pre-mature Adu
Pre-mature Juv
Mature Juv
Adult leaves: ≥ 8
Transition leaves: 5-7
Juvenile leaves: 1-4
Cotyledon (C)
2w
3-5w
6-8w
Senescence Juv

Figure S2

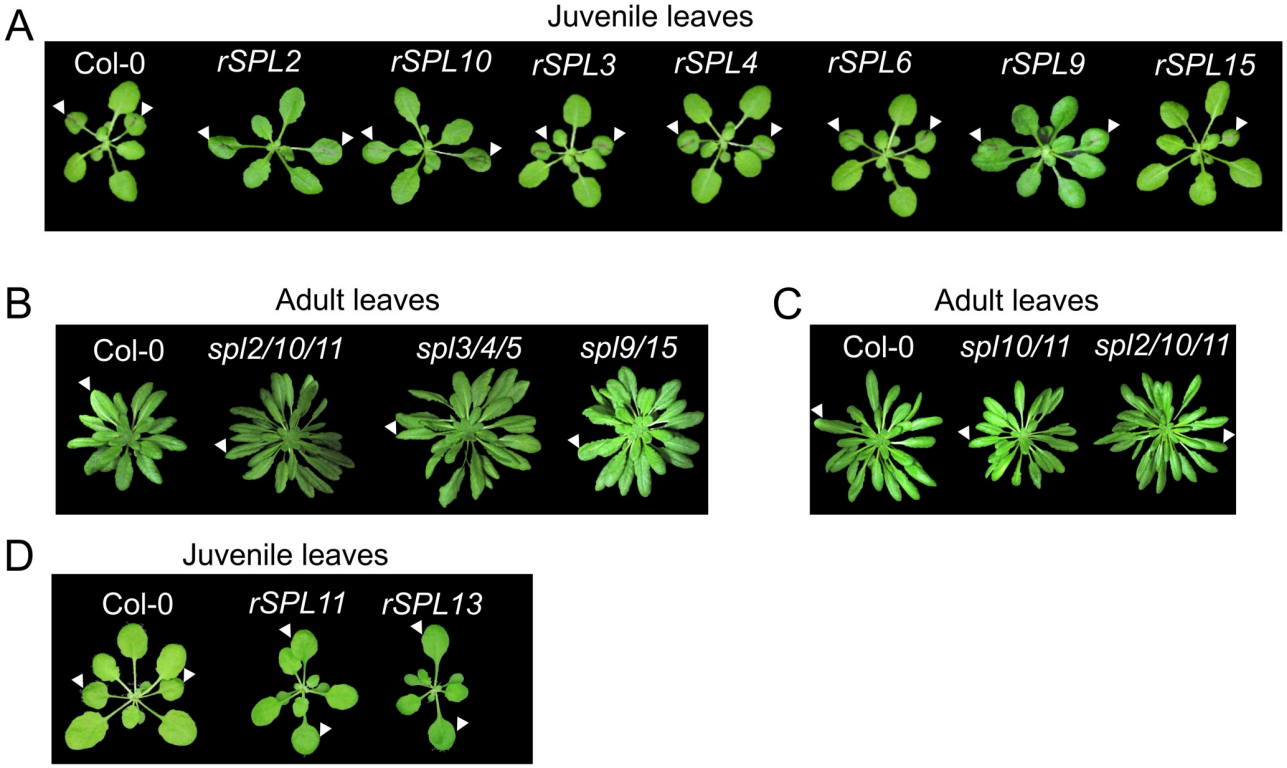
A
Juvenile leaves
Col-0
rSPL2
rSPL10
rSPL3
rSPL4
rSPL6
rSPL9
rSPL15
B
Adult leaves
Col-0
spl2/10/11
spl3/4/5
spl9/15
C
Adult leaves
Col-0
spl10/11
spl2/10/11
D
Juvenile leaves
Col-0
rSPL11
rSPL13

Figure S3

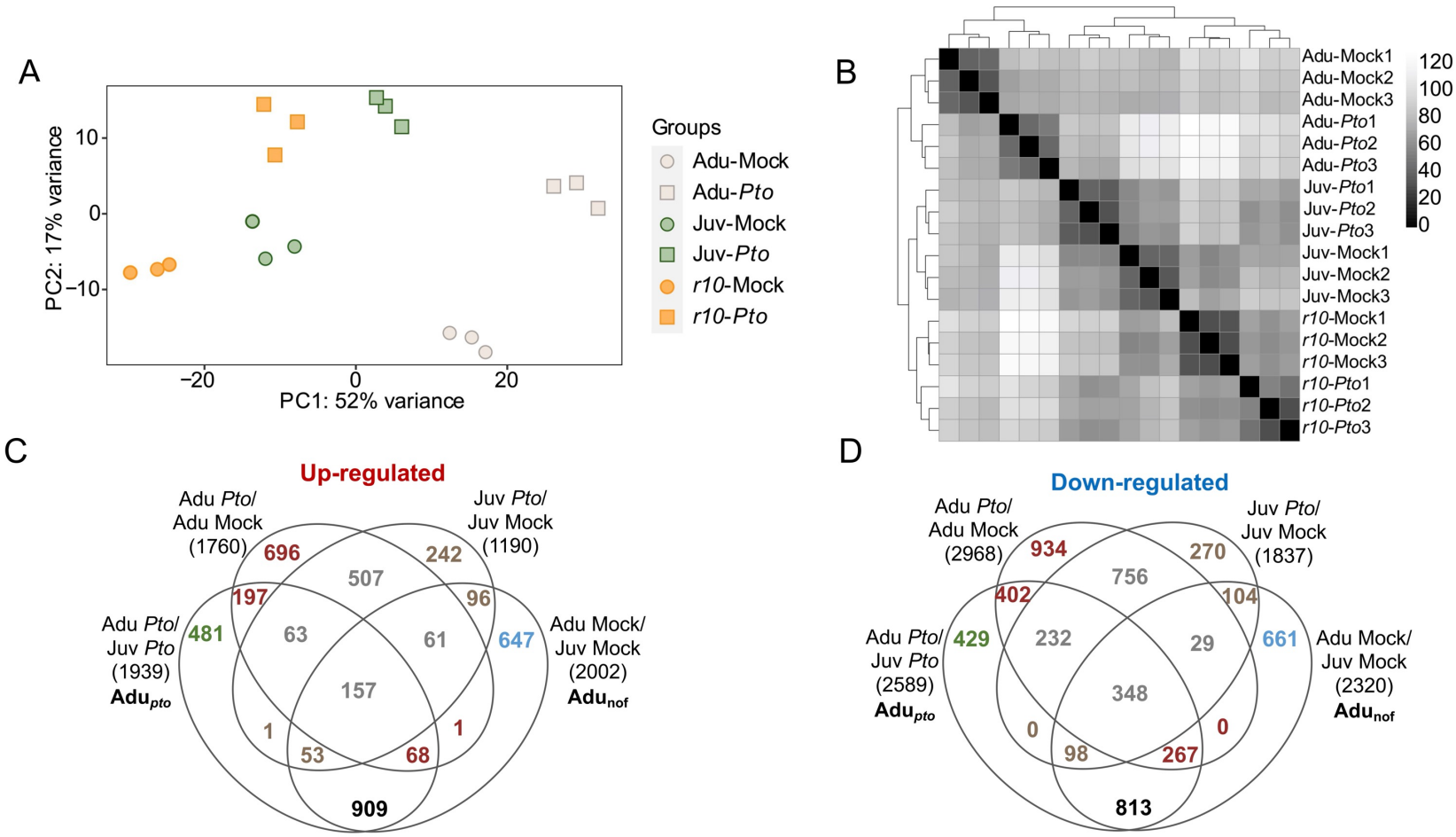
A
PC2: 17% variance
PC1: 52% variance
10
0
−10
−20
0
20
Groups
Adu-Mock
Adu-Pto
Juv-Mock
Juv-Pto
r10-Mock
r10-Pto
B
Adu-Mock1
Adu-Mock2
Adu-Mock3
Adu-Pto1
Adu-Pto2
Adu-Pto3
Juv-Pto1
Juv-Pto2
Juv-Pto3
Juv-Mock1
Juv-Mock2
Juv-Mock3
r10-Mock1
r10-Mock2
r10-Mock3
r10-Pto1
r10-Pto2
r10-Pto3
120
100
80
60
40
20
0
C
Up-regulated
Adu Pto/ Adu Mock (1760)
Juv Pto/ Juv Mock (1190)
Adu Pto/ Juv Pto (1939) Adupto
Adu Mock/ Juv Mock (2002) Adunof
696
242
507
197
96
481
63
61
647
157
1
1
53
68
909
D
Down-regulated
Adu Pto/ Adu Mock (2968)
Juv Pto/ Juv Mock (1837)
Adu Pto/ Juv Pto (2589) Adupto
Adu Mock/ Juv Mock (2320) Adunof
934
270
756
402
104
429
232
29
661
348
0
0
98
267
813

Figure S4

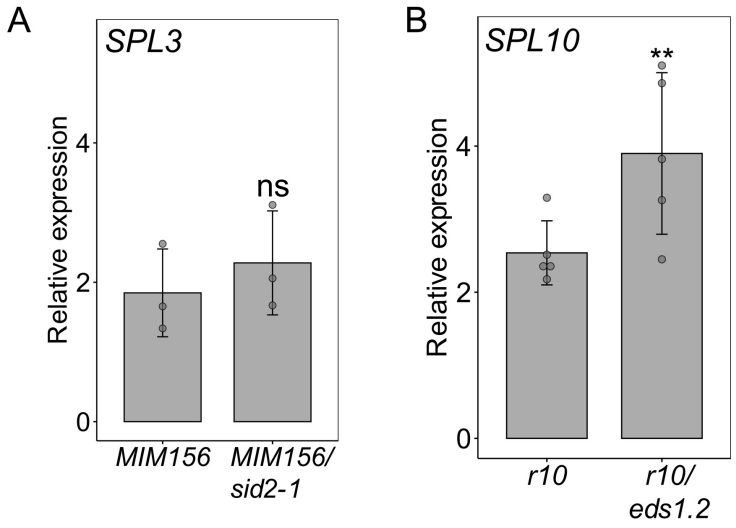
A
SPL3
Relative expression
0
2
4
ns
MIM156
MIM156/
sid2-1
B
SPL10
Relative expression
0
2
4
**
r10
r10/
eds1.2

Figure S5

A

Alt ID	P-value	E-value	Q-value (FDR)	TP (Primary seq Match to the motif)	FP (% control seq match to the motif)	Enrichment Ratio (Primary relative to control)	Threshold (set TP/FP)
SPL1	2.60e-4	2.27e-1	6.95e-3	25/183 (13.7%)	6/183 (3.3%)	3.71	12.56
SPL5	2.40e-3	2.1e0	2.69e-2	24/183 (13.1%)	8/183 (4.4%)	2.78	12.38
SPL15	3.69e-3	3.22e0	3.60e-2	29/183 (15.8%)	12/183 (6.6%)	2.31	9.14

B

Figure S6
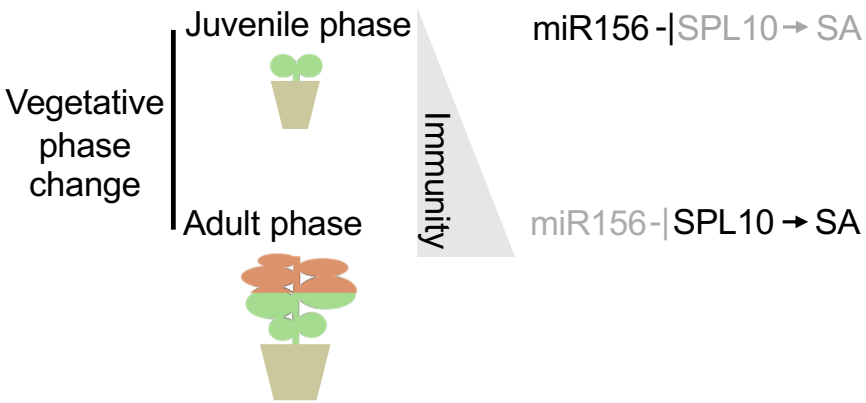
A working model of programming the age-related resistance.